Das **GeoTHERM Journal** ist eine von Experten begutachtete Zeitschrift, die der Veröffentlichung von wissenschaftlichen Erkenntnissen und praxistauglichen Beispielen der Erkundung und Nutzung von geothermischer Energie gewidmet ist. Der Leitgedanke entspricht dem Motto der GeoTHERM - expo & congress, der jährlich stattfindenden Ausstellung und Kongress in Offenburg, die Oberflächennahe und Tiefe Geothermie in allen Facetten darzustellen, die Potenziale und Vor- und Nachteile zu kommunizieren und eine Plattform zum Wissens- und Erfahrungsaustausch zu bieten.

Band 1, Jahrgang 2023

Publiziert:	15.12.2023
Autoren:	Referentinnen und Referenten desjährlichen GeoTHERM-Kongresses in Offenburg, Deutschland
Herausgeber:	Doherr, D. (Steinbeis-Transferzentrum IT, Schutterwald) Kircher, S. (Messe Offenburg-Ortenau, Offenburg)
Journal-Plattform:	Open Journal System PKP (Public Knowledge Project)
Webadresse:	https://geotherm-journal.com

In dieser GeoTHERM Journalausgabe enthaltene Artikel

Editorial Note

Herzlich willkommen zum ersten Jahrgang des "GeoTHERM-Journal“ – einem wegweisenden Open-Access-Journal, das sich der Veröffentlichung hochwertiger wissenschaftlicher und technischer Beiträge aus dem Bereich der Geothermie widmet. Dieses Journal ist das Ergebnis einer Zusammenführung herausragender Forschungsergebnisse, die im Rahmen der jährlich stattfindenden GeoTHERM-Konferenz in Offenburg präsentiert wurden.

Die GeoTHERM - expo & congress ist eine jährlich stattfindende Fachmesse mit begleitendem wissenschaftlichem Kongress, die die aktuellen Entwicklungen der Branche aufgreift und eine internationale Plattform schafft, die sich fachspezifisch und neutral mit den Möglichkeiten, Chancen und Risiken der Nutzung geothermischer Energie widmet. Damit besteht für Aussteller, Referenten und Besucher gleichermaßen die Möglichkeit, sich über neueste Entwicklungen zu informieren und sich im weltweiten Dialog auszutauschen.

Die in diesem Journal präsentierten Artikel basieren auf Vorträgen, die in einem strengen Qualitätssicherungsprozess im Rahmen des Double Blind Verfahrens von externen Expertinnen und Experten ausgewählt und begutachtet wurden.

Dieser Ansatz gewährleistet, dass die Beiträge objektiv bewertet wurden und höchsten wissenschaftlichen Standards entsprechen. Unsere engagierte Herausgeber- und Gutachtergemeinschaft trägt dazu bei, sicherzustellen, dass die veröffentlichten Arbeiten einen bedeutenden Beitrag zur Weiterentwicklung der Geothermie leisten und einen Meilenstein für die Verbreitung von Erkenntnissen im Bereich der geothermischen Exploration und Nutzung setzen.

Die Inhalte dieses Journals decken ein breites Spektrum ab, das von wissenschaftlichen Erkenntnissen über administrative Aspekte bis hin zu technologischen Neuerungen reicht. Wir legen besonderen Wert auf Beiträge, die sich mit der Erkundung geothermischer Potenziale befassen und gleichzeitig Strategien zur Risikominimierung bei der Aufsuchung und Anwendung dieser Ressourcen entwickeln. Diese Vielfalt spiegelt die multidisziplinäre Natur der Geothermie wider und trägt dazu bei, ein umfassendes Verständnis für die

Herausforderungen und Möglichkeiten in diesem Bereich zu schaffen.

Wir sind stolz darauf, dieses Journal mit offenem, kostenfreien Zugang für die globale Gemeinschaft anzubieten. Der ungehinderte Zugang zu wissenschaftlichen Erkenntnissen ist entscheidend, um den Fortschritt in der Geothermie-Forschung zu fördern und innovative Lösungen für eine nachhaltige Nutzung dieser erneuerbaren Energiequelle voranzutreiben.

Wir möchten allen Autorinnen und Autoren danken, die ihre Arbeit eingereicht haben, sowie den Gutachtern und Herausgebern, die ihre Expertise und Zeit eingebracht haben, um dieses Journal veröffentlichen zu können. Gern nehmen wir Ihre Anregungen und Hinweise entgegen, wenn wir Ihrer Meinung nach das Journal weiterentwickeln oder mit spezifischen Schwerpunkten erweitern sollen.

Gemeinsam freuen wir uns auf eine inspirierende Reise durch die Welt der Geothermie, in der wir dazu beitragen wollen, die Zukunft der nachhaltigen Energiegewinnung zu gestalten.

Vielen Dank für Ihr Interesse und Ihre Unterstützung!

Mit freundlichen Grüßen
Ihre Herausgeber
S. Kircher und D. Doherr

Prof. Dr. Detlev Doherr
Steinbeis-Transferzentrum IT
Mörikestr. 1
77746 Schutterwald

Sandra Kircher
Messe Offenburg-Ortenau GmbH
Schutterwälderstr. 3
777656 Offenburg

GeoWaermeWende - Empowering Low-Temperature District Heating and Cooling Networks with Comprehensive Geospatial Monitoring, Multi-Purpose Simulation Approaches, and User-Centric Planning Tools

Lukas Drexler[a], Linus Cuypers[a], Sebastian Weck-Ponten[a], Thomas Lemmerz [b], Fadi Moubayed [b], Aaron Förderer [c], Ralf Becker [b], Jérôme Frisch[a], Raul Fuentes [c], Jörg Blankenbach [b], Christoph van Treeck[a]

[a] Institute of Energy Efficiency and Sustainable Building E3D, RWTH Aachen University

[b] Chair of Building Informatics and Geoinformation Systems, RWTH Aachen University

[c] Chair of Geotechnical Engineering and Institute of Geomechanics and Underground Technology, RWTH Aachen University

1 ABSTRACT

Planning low-temperature district heating and cooling networks (LTDHCN) still poses many challenges. It requires research, especially in the scalability of the networks and the connected energy producers and heat sources. In the project GeoWaermeWende (project number 03EN3059), a passive, existing LTDHCN is monitored. For this purpose, a monitoring concept will be developed to collect relevant operating parameters at different network locations, which will be compiled and processed in a database. In addition, various tools are developed for planning LTDHCN. With the help of the measurement data, individual simulation models are validated, which provide the basis for a holistic district model consisting of all relevant components. Analytical and numerical approaches enable a variety of promising analyses regarding the network dynamics under changing boundary conditions and the interaction of the network with the subsurface. All simulation tools are accessed via a geothermal network information system (GNIS). The GNIS is established as a spatial data infrastructure with a geoportal to facilitate web-based access to the data required for the analysis and simulation. The geoportal is also

DOI: 10.53196/gtj-2023.1

to be used to configure and analyze the LTDHCN.

Keywords: GeoWaermeWende, LTDHCN, Thermal Network Simulation, Shallow Geothermal Energy, GIS, Geoportal

2 INTRODUCTION

The urgency for a rapid and decisive energy transition is increasingly apparent in the context of the escalating climate change. The need for action intensifies as the impacts of rising global temperatures on ecosystems and societies are evident. The building sector is responsible for a significant part of the total greenhouse gas emissions, highly emphasizing effort towards its decarbonization. Therefore, an urgent need to increase the usage of renewable energy sources as an alternative to fossil fuels in the building sector is evident.

Shallow geothermal energy is becoming increasingly recognized as a renewable energy source that can provide reliable energy for space heating, domestic hot water (DHW), and space cooling. Its base-load capability underscores its reliability, addressing concerns often associated with other renewable sources. Recently, Germany has been taking legislative steps to emphasize the importance of local heat planning and the transition to renewable energy sources in municipalities. The upcoming *Second Amendment of the Building Energy Act* is expected to have significant implications for implementing and expanding heating networks, including LTDHCN, in Germany. To make the most use of this technology's potential, building new and transforming existing heating networks is essential. In particular, LTDHCN offer an efficient way to utilize geothermal energy and are a practical method of distributing heat throughout a residential district. The passivity of the system without a central circulation pump makes the system more robust and easier to scale. However, estimating and controlling the hydraulic conditions and the associated quality of mutual heat exchange can be quite difficult.

Although the benefits of LTDHCN are widely recognized, their implementation can be challenging, especially for existing heating networks with a higher temperature level or districts with no heating network. Considering the complexity of the technology, it is crucial to develop an intuitive and user-friendly planning tool. This tool would simplify the planning and configuration processes and encourage the broader implementation of LTDHCN, which is a fundamental step toward sustainability.

DOI: 10.53196/gtj-2023.1

3 PROJECT DESCRIPTION

One core element of the project is the sensory equipment and the monitoring of the LTDHCN in the German city of Schifferstadt. The data collected in the monitoring process is used to validate simulation models, which represent a digital image of the actual model and are also used in planning new LTDHCN. This knowledge will be combined into a planning tool to support specialist planners in designing and analyzing new LTDHCN. In addition, an augmented reality app is being developed to visualize the heating network in Schifferstadt, making the technology accessible to a broader audience.

3.1 LTDHCN Schifferstadt

The LTDHCN in Schifferstadt is located in the Upper Rhine Plain in southwest Germany, a region with increased volcanic activity and the location of the Upper Rhine Aquifer. The geological conditions of this region give rise to many projects dealing with the extraction of geothermal heat.

In Schifferstadt, 41 residential buildings are thermally connected by an uninsulated heating network, as shown in Figure 1. The network consists of two meshes, each with a supply and a return loop. A geothermal borehole heat exchanger (BHE) field is connected in the district's northwest, consisting of 28 BHE with a drilling depth of about 95 meters each. The buildings are supplied by heat pumps that draw heat from the grid for heating purposes or feed heat back into the grid for cooling purposes. The heat pumps will collect analysis data since they are equipped with extensive sensor technology by their manufacturer to extract all relevant operation data. Additionally, various measuring points are planned at the maintenance building, the BHE, and at five positions inside the network. The sensors shall record the fluid's pressures, temperatures, and volume flows. All measurement data will be permanently stored in a database, processed, and made available for further use.

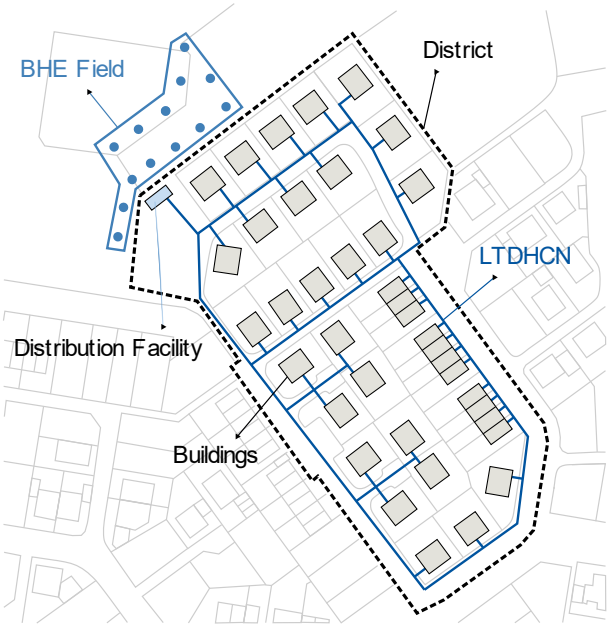

Figure 1: Schematic Floorplan of the LTDHCN in Schifferstadt

DOI: 10.53196/gtj-2023.1

3.2 Concept of the Overall Planning Tool

The entire planning tool is developed to enable web-based access by any interested party without installing additional software. This reduces barriers to using the tool and allows for quick results to be achieved. Depending on the planning stage, the requirements for the tools to be used and the level of detail of the results differ. Figure 2 shows the preliminary functional relationship of the different tools in the project.

The network information system (see Section **Fehler! Verweisquelle konnte nicht gefunden werden.**) compiles general data relevant to the planning of heating networks and passes it on to the system configurator (see Section **Fehler! Verweisquelle konnte nicht gefunden werden.**). System-specific parameters are defined there and passed on to the tools for modeling buildings, heat pumps, pipe networks, and underground. Both the simplified (blue) and the detailed models (red) will be triggered from the system configurator.

3.3 Geothermal Network Information System (GNIS)

The goal of the geothermal network information system (GNIS) adapted from a former project GeTIS ([1], [2]) is the establishment of a project-related spatial data infrastructure with a geoportal for web-based access to the data required in the analysis and simulation tools for the execution of these tools and, finally, for visualization of the obtained results.

The planning, dimensioning, and operational optimization of LTDHCN require various data.

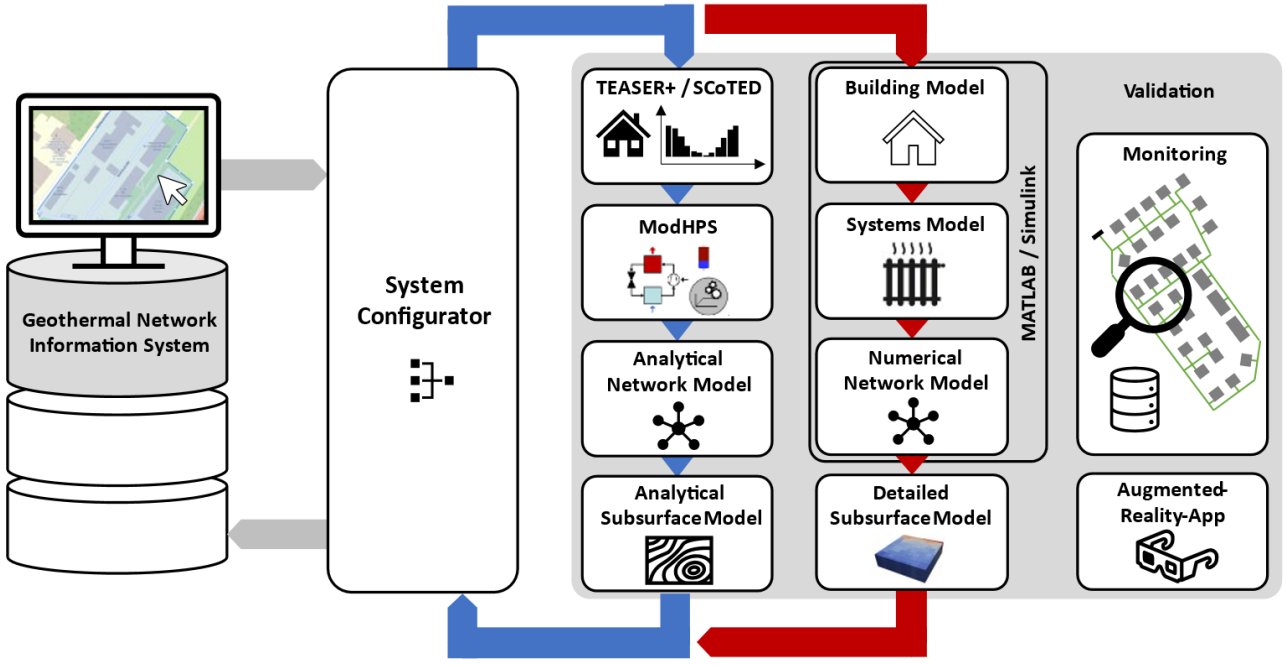

Figure 2: Conceptual flow chart of the toolchain to be developed

DOI: 10.53196/gtj-2023.1

An essential part of the spatial data infrastructure of the GNIS is the aggregation of hydrogeological data of the subsurface with data regarding the LTDHCN and semantic data of its environment. For this purpose, existing maps, subsurface and city models are linked with monitoring data and made available via the geoportal, as demonstrated in Figure 3. As far as possible, this data is connected to the GNIS via standardized interfaces of the Open Geospatial Consortium (OGC), such as the specified geodata services, also called OpenGIS Web Services (OWS). In this way, the data can be integrated into the GNIS but do not have to be transferred to a project-based, own database as a secondary dataset and are kept up to date automatically. Furthermore, it increases the interoperability and, thus, the scalability of the GNIS and improves the possibilities of further system development. The various analysis and simulation tools (see Section 0) can be connected to the geoportal via purpose-built interfaces based on the OpenGIS Web Processing Service (WPS) [3].

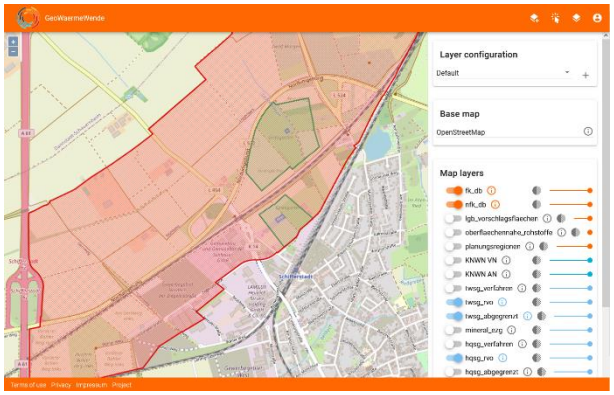

Figure 3: The Geoportal in GeoWaermeWende

This also includes interfaces for integrating georeferenced LTDHCN and the monitoring database. Furthermore, it is intended to incorporate planning and approval-relevant requirements and valuable information from real-world experience in the planning process of LTDHCN.

To fulfill the diverse demands, the GNIS is designed as a distributed geoinformation system (GIS) according to service-oriented architecture (SOA) principles. Corresponding to this principle, individual services are implemented and orchestrated to unite a large and powerful system that allows for flexible adaptation to new or changed requirements.

3.4 System Configuration

Following the digital geothermal site analyses and the data aggregation in the geothermal information system, the heat and cold generation systems and the LTDHCN must be designed. For a user-friendly design of the heat pumps, buffer, DHW storage tanks, and the network topology, the web-based system configurator GeoWPSys+Web [4] is used. GeoWPSys+Web gives automated system suggestions of available devices and provides default values for most design parameters. In GeoWaermeWende, the system configurator will be extended with functionalities for dimensioning and planning the LTDHCN routes. The resulting heat network

DOI: 10.53196/gtj-2023.1

configurator shall execute the calculation tools described in the following to determine or check design parameters automatically.

3.5 Calculation & Simulation

3.5.1 Simplified Approaches

Hourly load curves for heating, domestic hot water, and cooling are required to dimension a LTDHCN and the systems involved and input data for several models within the toolchain described here.

With the help of the open-source program TEASER+ [5], generic low-order Modelica building models can be parameterized, suitable for large-scale simulations of many buildings due to their low complexity. TEASER+ uses a database of archetypes, i.e., buildings with standard construction and usage profiles based on age and type, to scale building geometry based on net floor area, height, and number of floors or derives it from CityGML data, merging this with archetype data to create a reduced-order model. The models are refinable through additional parameters, with updated archetypes recently incorporated to better match the actual buildings in Schifferstadt.

Alternatively, the analytical tool SCoTED [6] can generate heating load curves by leveraging standard heating loads or annual energy consumptions of buildings, along with hourly weather data. Unlike TEASER+, SCoTED also produces domestic hot water consumption curves.

The simplified heat pump system model ModHPS [7] used the hourly load curves created with the previously described tools to represent the decentralized distributed heat pumps at the district level. ModHPS is an open-source black-box characteristic curve model with control mechanisms and storage balances for buffer and DHW storage tanks. It can be used for individual buildings or entire city districts and coupled bidirectionally to subsurface models.

3.5.2 Automated determination of the number of storeys in buildings

Building parameters such as the average floor height, the total floor area, the window-to-wall ratio, and the number of storeys critically influence building energy simulations [8]. Accurate physical building parameters are vital for these simulations [9], yet they are difficult to obtain on a large scale. Even though machine learning, artificial intelligence, and image processing algorithms have been utilized in energy simulations, their applications have been restricted to individual buildings. Thus, they cannot scale on an urban level [10]. This is why developing algorithms to extract building parameters on an individual and a large level is important.

DOI: 10.53196/gtj-2023.1

The recent surge in oblique aerial imagery, especially in German cities, is promising since these images make building facades visible, enabling the extraction of facade information. The growing usage of 3D city models, like CityGML data, aids in energy simulations by providing standardized 3D representations of urban objects.

CityGML data provides a standardized 3D representation of city objects, i.e., buildings, in different levels of detail [11]. Depending on the level of detail, CityGML data can include building parameters such as the number of storeys. However, this information is highly inconsistent and dependent on the data provider. Nevertheless, other important information, such as the 3D coordinates of the building, is already available in CityGML data (Figure 5). Combining this information with oblique aerial imagery (Figure 4) is a basis for an automatic approach to determining the number of building floors. The process begins by selecting an appropriate oblique image

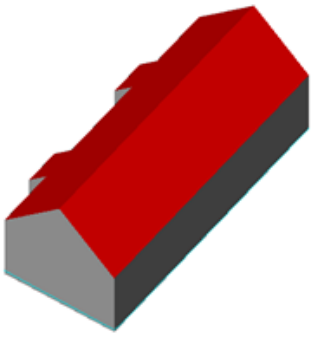

Figure 5: CityGML example viewed using FZK Viewer

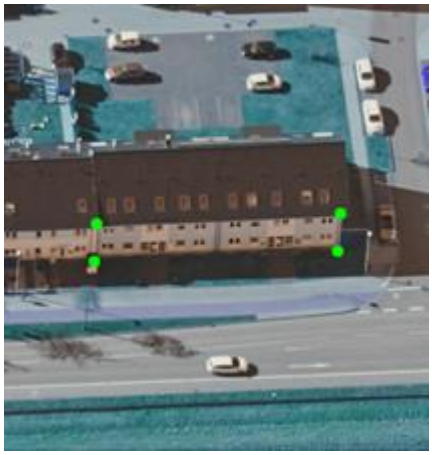

Figure 4: The corresponding facade in oblique aerial images (source: city of Soest, NRW Germany)

where a building's facade is clear. Utilizing 3D coordinates, the facade's location is pinpointed in the image, followed by facade rectification. Subsequent image processing identifies the edges representing windows on the facade. By analyzing the frequency of vertical edge pixels in each row of the image, it becomes feasible to calculate the building's number of floors based on the count of maxima in the frequency image.

3.5.3 Analytical ground and fluid models

A key to the adequate design of LTDHCN is to ensure sufficient and appropriate fluid temperatures within the network. Generally, the efficiency of a heat pump depends on both the temperature difference it needs to produce and the absolute fluid temperatures, showing a negative correlation with the former and a positive correlation with the latter. Furthermore, there is the need to assess the induced temperature changes in the

DOI: 10.53196/gtj-2023.1

subsurface to ensure the system's sustainability and conform to regulatory demands.

Therefore, the temperature of the fluids and the surrounding ground, need to be determined effectively. The chosen analytical approach divides the modeling area into two regions: The subsurface surrounding the heat exchangers (HE) and the area inside the heat exchanger. In this context, any system component with significant heat fluxes is considered a heat exchanger. That includes borehole heat exchangers (BHE) and the connecting network pipes.

The subsurface temperatures are determined through the construction of g-functions. Different boundary conditions are used for different system components: A constant temperature is commonly a boundary condition on the surface for borehole heat exchangers (BHE), modeled after [12]. Connecting pipes installed close to the surface are modeled using a time-dependent surface temperature boundary condition [13]. This allows the incorporation of daily and seasonal temperature cycles in areas above the neutral zone. Other types of heat exchangers can be integrated if a suitable g-function formulation is available.

After obtaining the g-functions for all system components, the temperature at the HE wall can be determined through

$$T_b = T_0 + \Delta T \quad (1)$$

where T_b and T_0 are the borehole and undisturbed ground temperature. For time-varying loads, the incremental load steps can be considered such that

$$\Delta T = \frac{1}{2\pi\lambda}\sum_{l=1}^{k}(q_l - q_{l-1}) \cdot g_{k-l+1} \quad (2)$$

where q is the thermal load, λ is the soil thermal conductivity and the g-function is a function of the characteristic time, radius, and buried depth of the BHE. This can be efficiently evaluated by computing the convolution of the load increment and g-function arrays [14].

T_b is linked to the circulating fluid temperature through the thermal resistance R_{th}, which encapsulates the heat transfer processes inside the HE. It is defined such that

$$\overline{T_f} = q \cdot R_{th} + T_b \quad (3)$$

where $\overline{T_f}$ is the average fluid temperature inside the HE.

Using R_{th} as a coupling parameter between HE and surrounding ground is advantageous due to its facilitation of a linear equation for complex heat transfer dynamics. This linearity, evident in Equations 1 and 3, aids in developing a linear system of equations for the system.

DOI: 10.53196/gtj-2023.1

System components are interconnected by equating the inlet and outlet fluid temperatures of successive HEs, as demonstrated in

$$T_{f,i,m} = T_{f,o,n} \quad (4)$$

These relations serve as constraints besides the total required heat load from the ground. The resulting system is expressed as a sparse matrix, which can be solved using SciPy's *sparse* algorithm [15], an approach validated by Düber et al. on systems involving BHE and corresponding pipes ([16], [17]).

The approach allows the incorporation of heat pump models such as ModHPS for additional fluid temperature and flow rate constraints, which are usually neglected in the conventional planning of such systems. The calculation times depend on the system complexity but should be in the minutes. This enables iterative or optimization algorithms to design the system for adequate fluid temperatures automatically.

3.5.4 Numerical Methods

The modeling and simulation of the hydraulic network, heat pumps, and buildings will be conducted in the SimScape [18] environment for detailed planning. SimScape is an extension of the Simulink software developed by Mathworks. It extends Simulink with graphical modeling of multiphysics systems in which individual sub-models can be interconnected via bidirectional signals. SimScape incorporates an extensive model library of individual components and provides examples of how these components can be implemented in complex systems. Therefore, it is suitable for modeling the changing flow direction in heat networks and the thermal interaction of the network with the subsurface. Although the CARNOT-toolbox [19] has proved unsuitable for use as the central platform in initial application trials, parts of it are nevertheless used for some subsystems of the numerical simulation model, such as for integrating weather data or calculating solar radiation.

Since the supply and return pipes of the network are usually located next to each other, a configurable double-pipe model is being developed to serve as a basic building block for a pipe section of any size. This allows the thermal interaction of the two conductors to be implemented within the model and the model structure to be simplified. The network is then composed of many double-pipe elements connected by T joints. In addition to the heat transfer, the pressure losses of the fluid are also calculated in this model.

The utilization of reduced-order models (ROM) is planned for the buildings, which are parameterized with the previously mentioned tool TEASER+. These models are based on the

DOI: 10.53196/gtj-2023.1

modeling approach of VDI 6007 [20] and an adaptation of Lauster et al. [21]. This guideline describes a calculation method based on the fundamental approach of considering the thermal zone as an electrical circuit. Each wall layer consists of a pair of resistances representing the thermal conductivity of the material and a capacitance representing the heat storage capacity. Several wall layers can be combined to form a wall element. The volume of air the walls enclose is assumed to be a homogeneous zone, resulting in an additional heat capacity. This air volume is extended by supply and exhaust air openings, which enables the implementation of ventilation flows. Heating and cooling effects and internal gains can be modeled via ideal sources and sinks and will be replaced in the further course of the project by modeling the system technology.

4 CONCLUSION

A comprehensive collection of activities has been defined in the project GeoWaermeWende, covering many theoretical, experimental, and modeling aspects of planning and operating a LTDHCN. The project addresses many areas of the subject of geothermally fed LTDHCN, such as gathering and processing georeferenced data relevant to system design and approval procedures, basic and applied understanding of hydraulic and thermodynamic behavior of heating networks, analytical and numerical modeling and validation, as well as involving the public and presenting scientific findings. Initial results over the first months of GeoWaermeWende have been encouraging and offer fresh insights. This wealth of new knowledge is expected to help municipalities, planning authorities, and other parties implement LTDHCN technology broadly.

5 ACKNOWLEDGEMENTS

The authors would like to thank the GeoWaermeWende partners and advisors for contributing to this paper. GeoWaermeWende (project number 03EN3059) is funded by the Federal Ministry for Economic Affairs and Climate Action.

6 REFERENCES

[1] R. Becker, M. Laska, and J. Blankenbach, “Webbasierte Geodaten- und Kommunikationsinfrastruktur für die Analyse geothermischer Energiesysteme,” *gis.Science*, pp. 148–160, Apr. 2022.

[2] C. Treeck *et al.*, “GeTIS - Geothermisches Informationssystem zur

Bemessung, Modellierung, Bewertung und Genehmigung vernetzter geothermischer Energiesysteme auf Gebäude- und Stadtquartiersebene : Schlussbericht," RWTH Aachen University, Lehrstuhl für Energieeffizientes Bauen (E3D), 2020. doi: 10.2314/KXP:1738225658.

[3] M. Laska, S. Herlé, J. Blankenbach, E. Fichter, and J. Frisch, "WhizPS: An architecture for well-conditioned, scalable geoprocessing services based on the WPS standard," Jan. 2019.

[4] S. Weck-Ponten, "Simulationsbasiertes Mehrebenen-Planungswerkzeug für geothermische Wärmepumpensysteme," Dissertation, RWTH Aachen University, 2023.

[5] A. Malhotra, M. Shamovich, J. Frisch, and C. van Treeck, "Parametric study of the different level of detail of CityGML and energy-ADE information for energy performance simulations," *Building simulation 2019*. IBPSA, Rome, Italy, pp. 3429–3436, 2019. doi: 10.26868/25222708.2019.210607.

[6] D. Koschwitz, M. A. Brüntjen, A. Chivite, J. Frisch, and C. A. Van Treeck, "Softwaregestützte Wärmebedarfsermittlung bei Informations- und Ressourcenknappheit," in *CESBP central european symposium on building physics / BauSIM 2016*, Dresden: Fraunhofer IRB Verlag, Sep. 2016.

[7] S. Weck-Ponten, J. Frisch, and C. van Treeck, "Simplified heat pump system model integrated in a tool chain for digitally and simulation-based planning shallow geothermal systems," *Geothermics*, vol. 106, p. 102579, Dec. 2022, doi: 10.1016/j.geothermics.2022.102579.

[8] S. Weck-Ponten, R. Becker, S. Herle, J. Frisch, J. Blankenbach, and C. A. Van Treeck, "Automatisierte Datenaggregation zur Einbindung einer dynamischen Gebäudesimulation in ein Geoinformationssystem," in *BauSIM 2018 : 7. deutsch-österreichische IBPSA Konferenz : Tagungsband*, P. V. Both, A. Wagner, and K. Graf, Eds., Karlsruhe: Karlsruher Institut für Technologie (KIT), Sep. 2018, pp. 516–523.

[9] A. S. Silva and E. Ghisi, "Uncertainty analysis of user behaviour and physical parameters in residential building performance simulation," *Energy Build.*, vol. 76, pp. 381–391, Jun. 2014, doi: 10.1016/j.enbuild.2014.03.001.

[10] A. Malhotra, M. Shamovich, J. Frisch, and C. Van Treeck, "Urban energy simulations using open CityGML models: A comparative analysis," *Energy Build.*, vol. 255, p. 111658, Jan. 2022, doi: 10.1016/j.enbuild.2021.111658.

[11] G. Gröger, T. H. Kolbe, C. Nagel, and K.-H. Häfele, “OGC city geography markup language (CityGML) encoding standard.” Open Geospatial Consortium, 2012.

[12] M. Cimmino, “Semi-Analytical Method for g-Function Calculation of bore fields with series- and parallel-connected boreholes,” *Sci. Technol. Built Environ.*, vol. 25, no. 8, pp. 1007–1022, 2019, doi: 10.1080/23744731.2019.1622937.

[13] L. Lamarche, “Horizontal ground heat exchangers modelling,” *Appl. Therm. Eng.*, vol. 155, pp. 534–545, 2019, doi: https://doi.org/10.1016/j.applthermaleng.2019.04.006.

[14] D. Marcotte and P. Pasquier, “Fast fluid and ground temperature computation for geothermal ground-loop heat exchanger systems,” *Geothermics*, vol. 37, no. 6, pp. 651–665, 2008, doi: https://doi.org/10.1016/j.geothermics.2008.08.003.

[15] P. Virtanen *et al.*, “SciPy 1.0: Fundamental algorithms for scientific computing in python,” *Nat. Methods*, vol. 17, pp. 261–272, 2020, doi: 10.1038/s41592-019-0686-2.

[16] S. Düber, R. Fuentes, and G. A. Narsilio, “Comparison and integration of simulation models for horizontal connection pipes in geothermal bore fields,” *Geotherm. Energy*, vol. 11, no. 15, p. 32, Jun. 2023, doi: https://doi.org/10.1186/s40517-023-00252-8.

[17] S. Düber, R. Fuentes, and G. Narsilio, “Effect of horizontal connection pipes on operation of borehole heat exchangers under different climatic conditions,” *Geothermics*, vol. 110, p. 102679, 2023, doi: https://doi.org/10.1016/j.geothermics.2023.102679.

[18] The MathWorks, Inc., “SimScape.” Jan. 2023.

[19] Solar-Institut Juelich, “CARNOT Toolbox.” 2022.

[20] VDI, “VDI 6007 Blatt1: Berechnung des instationären thermischen verhaltens von räumen und gebäuden.” Beuth Verlag GmbH, 2015.

[21] M. Lauster *et al.*, “Improving a low order building model for urban scale applications,” in *Fifth german-austrian IBPSA conference*, Sep. 2014.

Fast Calculation Method for Borehole Heat Exchanger Fields in Groundwater Flow

Roland KOENIGSDORFF, Lukas SCHLEICHERT, Adinda VAN DE VEN

Institute of Building and Energy Systems, Biberach University of Applied Sciences

D-88400, Biberach a. d. Riß

Germany

ABSTRACT

One class of methods for the design of borehole heat exchanger fields is the use of analytical, non-dimensional thermal step responses, such as g-functions. A main simplification and restriction of most such analytical approaches for BHE design is the neglection of groundwater advection.

The theory and concept of moving line sources can, in principle, be used to calculate the thermal behaviour of BHEs in groundwater flow. However, application of the moving line source to grouted boreholes needs a correction for the disturbance of the groundwater flow field and the lower heat transfer rates in the borehole region.

Based on such a correction developed earlier, the applicability of the infinite moving line source model on borehole fields is shown by comparison with numerical simulation. Together witch spatial superposition of the long-term temperature responses and influences, fields of arbitrarily placed borehole heat exchangers can be calculated. This yields an analytical, simple and fast calculation method for borehole heat exchanger fields with the boreholes being completely (or at least mainly) immersed in flowing groundwater.

A design example is presented, in which one of three borehole heat exchangers can be saved when a significant groundwater flow is present and taken into account.

Keywords: borehole heat exchangers, analytical line source models, thermal interference, groundwater advection**.**

DOI: 10.53196/gtj-2023.1

1. INTRODUCTION

The design of vertical borehole heat exchangers (BHEs) for ground source heat pumps (GSHP) and direct geothermal cooling requires calculation of the thermal response of the BHEs to the thermal loads imposed. Since the system of BHEs and surrounding ground coupled to them exhibits a transient thermal behaviour and is subject to time-dependent loads, appropriate dynamic calculation methods are necessary for dimensioning.

The calculation methods used are either numerical simulations, or (semi-)analytical mathematical models [1]. Accurate numerical simulations for BHE fields, especially when a large number of are BHEs has to be considered, are highly flexible but expensive in terms of computer power and calculation time. Established analytical calculation for BHE fields are simple and fast, but they include conceptual simplifications und thus are only valid for particular conditions [1]. One main simplification and restriction of most existing tools for BHE design, such as EED [2], is the neglection of groundwater advection.

The theory and concept of infinite and finite moving line sources can be used to calculate the thermal behaviour of BHEs in groundwater flow. But in the case of grouted boreholes, which are mandatory in many countries and regions, the original moving line source theory may fail in many cases, since it assumes a homogenous ground with constant permeability [1].

This article describes the application of a simple and fast calculation method for BHE fields consisting of grouted boreholes which are completely embedded in a homogenous groundwater flow.

2. ANALYTICAL MODEL

The base of the analytical model used here is the infinite moving line source (IMLS) [3]. Since the influence of a groundwater flow on the thermal response of a BHE under thermal loads is most pronounced in the long-term, groundwater flow is considered for the steady-state solution. The steady-state g-function, i.e. the stationary non-dimensionless temperature response, resulting from the IMLS is given by:

$$g_{GW,End,IMLS}(Pe) = I_0\left(\frac{Pe}{2}\right)\ K_0\left(\frac{Pe}{2}\right) \quad (1)$$

To take the grouting, i.e. the very much lower permeability within the borehole, into account, a correction function for the borehole wall temperature calculated from the IMLS was developed in a former work [1]:

$$f_{cor}(Pe) = -6.11 \cdot 10^{-3} \cdot Pe^2 + 3.68 \cdot 10^{-1} \cdot Pe + 1 \quad (2)$$

Figure 1 shows a comparison of the original steady-state groundwater g-function and the corrected function in dependence of the Péclet

DOI: 10.53196/gtj-2023.1

number *Pe*.

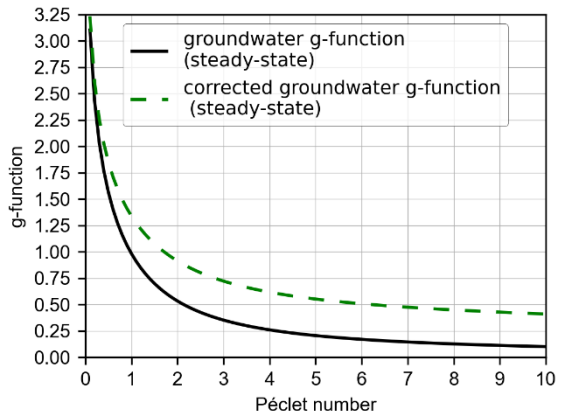

Fig. 1: Steady-state groundwater g-function with and without correction for the grouted borehole (taken from [1])

With equations (1) and (2) the steady-state temperature response at the borehole wall (averaged over the borehole wall) of a single BHE to a constant thermal load can be calculated:

$$\Delta T = \frac{\dot{q}}{2 \cdot \pi \cdot \lambda} \cdot \left(f_{cor}(Pe) \cdot g_{GW,End,IMLS}(Pe) \right) \quad (3)$$

For design and dimensioning purposes, only maximum resulting temperature responses of the fluid temperature within the BHE are needed. Therefore, a calculation or simulation of the whole time-dependent temperature response may be replaced by a transient calculation which aims directly on the design point (maximum and minimum fluid temperatures) [4-7].

The calculation of the response of a whole BHE field completely embedded in groundwater flow to a transient thermal load profile is then based on three assumptions:

1. Established calculation methods for the borehole resistance R_b of the grouted boreholes or values obtained from a short-term thermal response test are still applicable under groundwater advection.
2. A correction of the temperature field calculated with the IMLS is necessary at the borehole wall because of the backfilling of the borehole, but can be omitted at a greater distance from the borehole.
3. For a fast, simple and approximate, but sufficiently accurate calculation method for practical engineering purposes, consideration of groundwater advection can be limited to the steady-state part.

While the validity of the first assumption has already been shown in [1], assumptions 2 and 3 are discussed in the following sections.

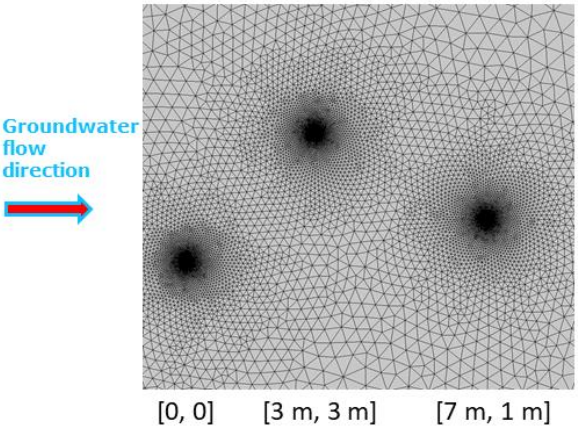

Fig. 2: Finite element grid of the numerical simulation model

DOI: 10.53196/gtj-2023.1

3. NUMERICAL SIMULATION

A test case of a BHE field with three boreholes was simulated with COMSOL Multiphysics® software V6.1. The model and the simulations were 2D and steady-state. Fig. 2 shows the positions of the boreholes and the finite-element grid used with a very fine grid near the boreholes, and a coarser grid in between. Each test case was simulated twice, first with a permeable borehole (borehole region identical to surrounding, permeable ground) and second with a grouted borehole (borehole region impermeable). Results of both, permeable and grouted borehole, for Pe = 0.55 are depicted in Fig. 3 and Fig. 4. Fig. 5 shows the relative deviation of both calculations.

It can be seen, that in the case shown here, the resulting temperature field around the boreholes is only influenced by the grouting in the near-field around the boreholes, i.e. within a radius in the order of 1 m. Only there the rel. deviation is larger ±1% and for that reason displayed in white without coloured marking.

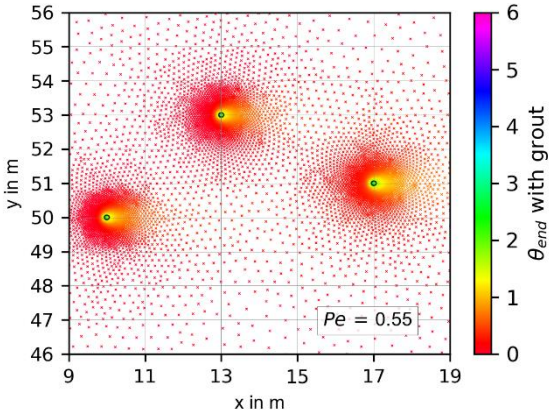

Fig. 3: Dimensionless temperature response for grouted boreholes

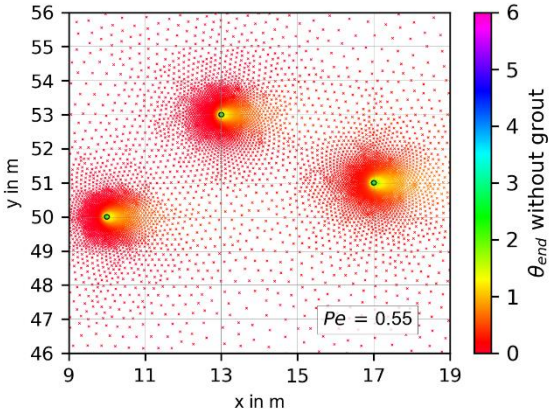

Fig. 4: Dimensionless temperature response for ungrouted boreholes

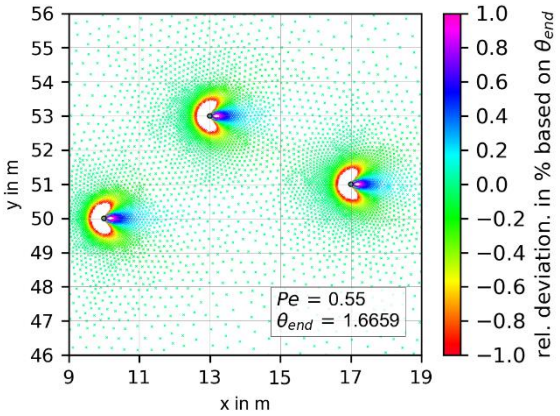

Fig. 5: Relative deviation of the dimensionless temperature response with and without grouted boreholes

DOI: 10.53196/gtj-2023.1

4. BHE FIELD STEADY-STATE G-FUNCTIONS

From the results of the numerical calculations it can be concluded that, while the correction according to equation (2) has to be applied at the borehole wall, no such correction is necessary in the far-field. This means that the analytical IMLS solution can be applied to calculate the thermal influence of one borehole on another within a BHE with groundwater flow field, even for grouted boreholes. For steady-state, this can be done with the angle and radius dependent IMLS solution:

$$\Delta\vartheta = \frac{\dot{q}}{2\ \pi\ \lambda_{eff}} \left\{ e^{\frac{Pe}{2}\ cos(\varphi)}\ K_0\left(\frac{Pe}{2}\right) \right\} \qquad (4)$$

with: $Pe = \frac{U_{eff}\ r_b}{\alpha_{eff}}$ (5)

The average steady-state g-function of the complete BHE field is then obtained by spatial superposition of the thermal influences between all BHEs and averaging the resulting values of all BHEs. The according angels and radii of the pairs of boreholes can easily be calculated from the horizontal coordinates of the boreholes (as given in Fig. 2 for the example investigated here). The procedure of superposing temperature responses and influences of arbitrarily located vertical BHEs is outlined in [8] where it is applied to BHE fields without groundwater influence.

5. TRANSIENT BEHAVIOUR APPROXIMATION

So far, stead-state conditions have been considered. However, in case of time-dependent thermal loads on the BHE field, a transient calculation of the thermal response of the underground an the BHEs has to be conducted. This is done by load decomposition according to the calculation method and software GEO-HAND^{light} which is originally based on analytical solutions given by Eskilson [4] and was further developed over the years [5].

The decomposition of a thermal load profile according to this method results in three components (and three thermal responses, accordingly):

a) steady-state, i.e. average load over the year (corresponding to the annual amount of thermal load),

b) periodic, i.e. seasonal component by using the maximum monthly average load, and

c) short-time constant load representing maximum heat load and duration (e.g. of a single GSHP operating phase).

Yet, GEO-HAND^{light} can only treat purely conductive heat transfer in the ground. The extension introduced here is the use of an average steady-state g-function with groundwater advection for component a), as described in the previous section. Periodic and

DOI: 10.53196/gtj-2023.1

short-time constant components, b) and c), are still calculated without groundwater advection as an approximation.

To obtain some picture of the accuracy of the latter approximation for components b) and c), g-functions calculated with the infinite line source ILS (pure conduction like in standard evaluation of a thermal response test) the transient IMLS, and the steady-state value of the IMLS are plotted in Fig. 6. In this example, steady-state under groundwater flow with *Pe* = 0.55 is reached already within 5 days. The maximum deviation between a response function composed of ILS and steady-state IMLS (red dashed lines in Fig. 7) and the more accurate transient IMLS is approximately 16%. Therefore, the treatment of components b) and c) is maintained without groundwater advection as a first approximation. However, when the g-functions without groundwater advection yield larger values than the steady-state IMLS, the latter is used for the respective component.

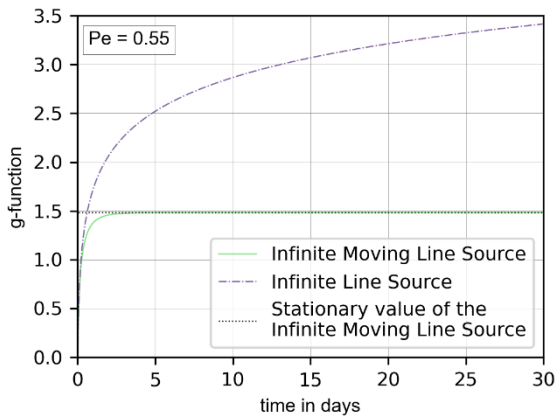

Fig. 6: Comparison of infinite line source and infinite moving line source for Pe = 0.55, linearly plotted over time in days

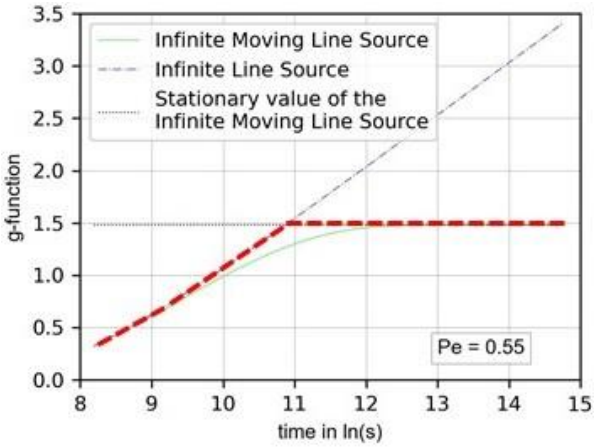

Fig. 7: Comparison infinite line source and infinite moving line source for Pe = 0.55, plotted over logarithmic time scale

6. DESIGN EXAMPLE

The design example listed in table 1 demonstrates the capability of the fast calculation method presented here. Two cases are compared: case I without groundwater flow and case II with a homogenous groundwater advection over the complete BHE field.

DOI: 10.53196/gtj-2023.1

Table 1: Parameters for the design example

heat pump properties:		
heat capacity	6	kW
COP	4.5	
SCOP	4.5	
Annual full load hours	1800	h/a
max. monthly full load hours	300	h/mon
max. uninterrupted operation hours	10	h
geology:		
thermal conductivity of the solid	2.0	W/(m·K)
thermal conductivity of the groundwater	0.6	W/(m·K)
porosity	0.3	
effective thermal conductivity	1.6	W/(m·K)
annual mean surface temperature	10	°C
Darcy velocity (case II only)	0.275	m/d
Péclet number (case II only)	0.55	
BHE properties:		
number of BHEs	3	
borehole depth	50	m
borehole radius	0.065	m
borehole resistance	0.08	m·K/W
temperature spread over the BHE	3	K

The resulting maximum heat extraction rate is 31.1 W/m borehole length. The long-term minimum inlet temperature to the borehole field is -3.1 °C in case I (no groundwater flow) and +2.4 °C in case II (with advection). Theses values correspond to a temperature decrease versus the undisturbed ground temperature of -14 K and -8.5 K, respectively. Given -3 °C as a limit, like it is the case in the German federal state of Baden-Württemberg [9], for example, the three BHEs are just sufficient when there is no groundwater flow, but only two BHEs would be sufficient if the groundwater flow is present over the hole depth of the BHE field.

7. SUMMARY AND CONCLUSIONS

The presented analytical fast calculation method extends the already established (semi-) analytical models for the design of BHE fields to the case with significant groundwater when it is present over the entire height of the BHE field. Through the comparison with numerical simulations, it is shown that the correction function for grouted boreholes published in [1] is only necessary in the near-field of the considered BHE, i.e. within a radius of 1 m around the BHE. Thus, the interference of BHEs can be calculated with the infinite moving line source solution without any correction. Since the presented method uses the load decomposition, which besides the long-term

DOI: 10.53196/gtj-2023.1

thermal interference and temperature decrease also considers the time-dependent, periodical and peak loads, in the latter cases the ILS solutions are used as long as these values are lower as the steady-state solution of the IMLS. This simplification leads to inaccuracies compared to the transient IMLS solution, while always being conservative concerning the temperature forecast. Despite of being somehow conservative in the present state on development, a design example shows the advantage, i.e. a reduction of 30% of the needed drilling meters, if the influence of a groundwater flow can be considered with this design method.

Since analytical simulation and design methods like the one presented here need only little computing time, they are well-suited for potential analysis over large regions, design of energy systems for whole building districts, and for integration into complex plant and building simulations.

Further development of the approach presented here is prepared, such as extension on stratified ground with different layers, e.g. with and without groundwater flow. Also, coupling with other shallow geothermal systems shall be developed.

8. REFERENCES

[1] A. Van de Ven, R. Koenigsdorff, P. Bayer (2021): “Enhanced Steady-State Solution of the Infinite Moving Line Source Model for the Thermal Design of Grouted Borehole Heat Exchangers with Groundwater Advection”, Geosciences 11 (10), 410.

[2] Blocon AB (2020): “EED version 4 - Earth Energy Designer: Update manual.” https://www.buildingphysics.com/manuals/EED4.pdf.

[3] M. G. Sutton., D.W. Nutter, R.J. Couvillion (2003): “A Ground Resistance for Vertical Bore Heat Exchangers With Groundwater Flow”, Journal of Energy Recources Technology 125, 183–189.

[4] P. Eskilson (1987): “Thermal analysis of heat extraction boreholes”. PhD. Thesis, Lund, Sweden.

[5] Download GEO-HAND^{light} (2023/09/28), HBC: https://form.hochschule-bc.de/ghl/

[6] R. Koenigsdorff (2011): „Oberflächennahe Geothermie für Gebäude: Grundlagen und Anwendungen zukunftsfähiger Heizung und Kühlung“. Fraunhofer IRB-Verlag,

DOI: 10.53196/gtj-2023.1

Stuttgart, 332 pp.

[7] J. M. Miocic, M. Krecher (2022): “Estimation of shallow geothermal potential to meet building heating demand on a regional scale”. Renewable Energy 185, 629–640.

[8] J. Miocic, L. Schleichert, A. Van de Ven, R. Koenigsdorff (2023/2024): “Fast calculation of the technical shallow geothermal energy potential of large areas with a steady-state solution of the finite line source”, accepted for publication in Geothermics.

[9] Ministerium für Umwelt, Klima und Energiewirtschaft Baden-Württemberg (2019) „Leitlinien Qualitätssicherung Erdwärmesonden: LQS EWS“. https://um.baden-wuerttemberg.de/de/energie/erneuerbare-energien/geothermie/lqs-ews/.

9. ACKNOWLEDGMENT

LS was funded within InnoSÜD, a project of the Innovative University Programme funded by the Federal Ministry of Education and Research (BMBF) and the participating states, grant number 03IHS024. AV is funded by the German Federal Ministry of Economic Affairs and Climate Action (BMWK) within the framework of the research project Quality Enhancement of Shallow Geothermal Systems (QEWSplus), grant number 03EE4020A. The authors gratefully acknowledge the financial supports given.

Die Leistungsfähigkeit der neuen Ringrohr-Erdwärmesonde und des ModX-Softwarepaketes – Messwerte und Simulation im Vergleich

Dipl.-Ing. Sebastian Paulo (RRS Geotherm, Freiberg)

Dipl.-Ing. Sadko Meusel (Transflow GmbH, Freiberg)

Prof.i.R. Dr.-Ing. Frieder Häfner (TU Bergakademie Freiberg)

Dr.-Ing. Rolf Michael Wagner (BLZ Geotechnik GmbH, Gommern)

KURZFASSUNG

Die hochleistungsfähige Ringrohr-Erdwärmesonde, die derzeit von den Unternehmen BLZ Geotechnik GmbH und Transflow Prozesstechnik GmbH in den Markt eingeführt wird, bietet die Möglichkeit, den Wärmeertrag gegenüber den traditionellen U-Sonden um mehr als 30% zu steigern. Kern der Neuentwicklung ist die Vergrößerung der wärmeaufnehmenden Fläche und sichere Verfüllung durch das patentierte Verfüllnetz, in dem 10 dünnwandige PE-Rohre mit 16 mm Außendurchmesser und ein 40 mm Aufstiegsrohr angeordnet sind. Innerhalb dieser Neuentwicklung wurden die Simulationsprogramme ModThermWg für die Planung und ModTRT für die Interpretation von Thermal Response Test entworfen, die mit einem 3-D numerischen Berechnungsgitter alle Sondentypen (U-Typen, Koaxial- und Ringrohr-Typen) ohne analytische Vereinfachungen erfassen.

Im Vortrag werden die Messwerte einer Anlage, die aus 3 EWS ein mehrgeschossiges Wohnhaus versorgt, die im gesamten Jahr 2022 gewonnen wurden, vorgestellt. Sie erlauben den Vergleich von Ringrohrsonde mit Verfüllnetz, ohne Verfüllnetz und Doppel-U-Sonde unter gleichen Bedingungen im Winter- und Sommerbetrieb. Diesen Messungen werden Simulationsergebnisse beigefügt, die die gute Nachbildung der tatsächlichen Leistung nachweisen.

Die Ringrohrsonde erweist sich insbesondere im kombiniertem Wärme- und Klimakältebetrieb als besonders vorteilhaft und erreicht Mehrleistungen gegenüber Doppel-U-Sonden bis zu 60%. Diese

DOI: 10.53196/gtj-2023.1

Eigenschaft macht sie besonders geeignet für kalte Nahwärmenetze, die in der Sommer- und Übergangszeit stundenweise bzw. auch monatelang industrielle Abwärme einspeichern müssen.

Zur Illustration werden Vergleiche von Mess- mit Simulationsdaten gezeigt.

EINLEITUNG

Die oberflächennahe Geothermie ist ein wichtiger Baustein zur Energiewende und wird mit vermutlich mittelfristig steigenden Stromkosten weiter an Bedeutung zunehmen. Aktuell sind die Kapazitäten der Bohrunternehmen voll ausgeschöpft. Dies spiegelt sich auch in den stark gestiegenen Preisen je Bohrmeter bzw. für die gesamte Geothermieanlagen wider. Generell unterliegen Bauprojekte einem enormen Kostendruck, welcher auch zu Lasten von Geothermieprojekten geht. Die Anlagen werden weniger leistungsfähig ausgeführt oder entfallen komplett.

Hier setzt im Bereich der Zirkulationssonden die neuartige Ringrohrsonde (RRS) [1] an, die mit mindestens einem Drittel weniger Bohrmetern die gleiche Leistungsfähigkeit wie die herkömmliche Doppel-U-Rohrsonden-Technologie (32x2,9) besitzt. Insgesamt ist eine Kosteneinsparung von ca. 30 % möglich.

KURZBESCHREIBUNG DER RINGROHRSONDE (RRS)

Die RRS setzt sich aus 10 Ringrohren (16x1,5), angeordnet um ein Zentralrohr (40x3,7), zusammen. Ein Sondenkopf verteilt den Zulauf gleichmäßig auf die Ringrohre, ein Sondenfuß führt die Ringrohre dann in einem Zentralrohr zusammen. Die Ringrohre sind an ihrer Außenseite mit einem Gewebeschlauch verklebt. Anschließend wird die Sonde gebündelt und ähnlich der Doppel-U-Rohrsonden eingebaut. Bei der Verfüllung wird der Gewebeschlauch, vom Sondenfuß beginnend, aufgeweitet und nimmt die Ringrohre mit sich an die Bohrlochwand. Die Position der Ringrohre und des Zentralrohrs sind nun im Bohrloch fest definiert.

Daraus ergeben sich bezogen auf die Doppel-U-Rohrsonde folgende Vorteile:

- (fast) direkter Kontakt zum Erdreich minimaler Wärmeübergabewiderstand
- 25 % mehr Rohroberfläche zur Aufnahme von Wärme
- minimaler thermischer Kurzschluss bzw. maximaler Abstand zwischen ab- und aufsteigenden Rohren
- kein preisintensives, thermisch hochleitfähiges Verfüllmaterial

DOI: 10.53196/gtj-2023.1

erforderlich, da der Wandabstand gering ist.

Hieraus folgt ein wesentlich geringerer thermischer Bohrlochwiderstand.

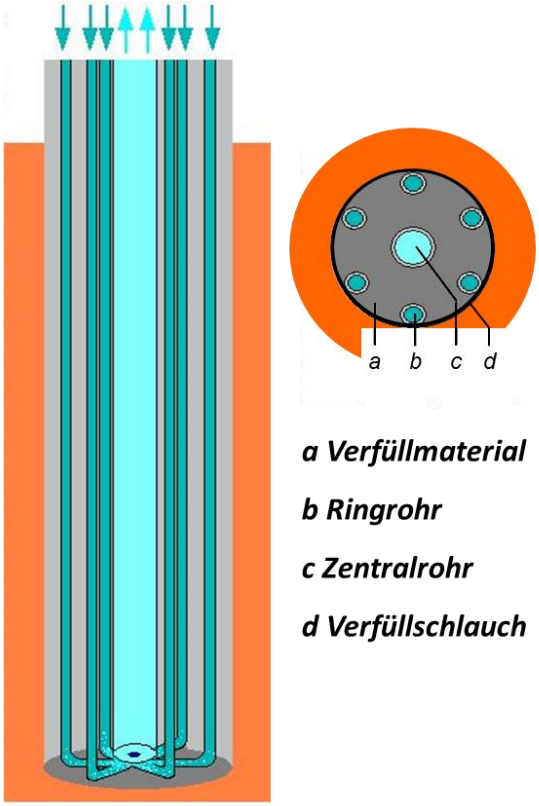

Abbildung 1: Prinzipaufbau einer Ringrohrsonde, nach [1]

Weitere Vorteile sind:

- erhöhte Verfüllqualität (keine Vermischung von Verfüllmasse mit Erdreich und Bohrspülung),
- Überbrückung von kleineren Hohlräumen / Klüften und somit Minimierung von Verfüllmaterialeinsatz und
- bestmögliche Trennung von Erdschichten und Grundwasserleitern.

Die Entwicklung der Ringrohrsonde wurde mittels Simulation begleitet. Bezogen auf eine Bohrung mit 150 mm, stellen 10 Rohre in der Dimension D16 ein Optimum dar. Mehr Rohre werden keine relevante Verbesserung der Leistungsfähigkeit nach sich ziehen, weniger Rohre verschlechtern diese aber deutlich.

KURZBESCHREIBUNG DES MODX-SOFTWAREPAKETES

Um zu ermitteln, welche Erdwärmesonde für den entsprechenden Anwendungsfall und Bedarf erforderlich ist, gibt es vereinfachende und komplexere Berechnungshilfen. Vereinfachende Berechnungshilfen arbeiten mit Kennfeldern / Tabellen, etwas komplexere mit analytischen Formeln mit im Anwendungsbereich akzeptablen Abweichungen und sehr genaue mit numerischen Berechnungsverfahren.

Für die RRS sind numerische Berechnungsverfahren mit dem ModX-Softwarepaket (ModThermWg, ModGeo3D, ModTRT) verfügbar. Sie bauen auf der gleichen mathematisch-numerischen Logik auf, sind aber für ihre jeweiligen Einsatzgebiete konzipiert (in dreidimensionalen Zylinder- bzw. kartesischen Koordinaten).

DOI: 10.53196/gtj-2023.1

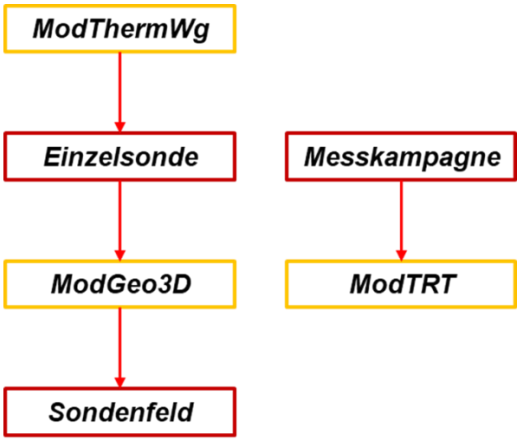

Abbildung 2: Prinzipschema des ModX-Softwarepaketes

ModThermWg simuliert den Wärmetransport zwischen Erdreich und einer Einzelsonde. Hierbei sind Eingangsparameter wie Sondentyp und -abmessungen, Bodenwärmeleitfähigkeit und andere Bodeneigenschaften, Grundwasserströmung, thermische Leistung, Jahresarbeitsstunden, Kühlung und andere Parameter anzugeben.

ModTRT wird für die Auswertung des (Geo)Thermal Response Tests (TRT) eingesetzt, sowohl für RRS als auch für die gängigen Erdwärmesondentypen. Die erforderlichen Eingangsparameter werden im TRT gemessen und bereitgestellt.

Für eine Sondenfeldberechnung kommt *ModGeo3D* hinzu. Es nutzt die Simulation für Einzelsonden aus ModThermWg und wendet diese auf einen im 3D-Schema definierten Erdkörper an. Hierbei ist es unerheblich, ob alle Erdwärmesonden (EWS) im Sondenfeld gleich sind oder ob jede EWS eine eigene Dimension und einen eigenen Typ aufweist.

Das ModX-Paket arbeitet ohne analytische Vereinfachungen, sondern mittels numerischer Lösungen der Wärmetransportgleichungen im 3D-Raum in jedes und in/aus jedem Einzelrohr in seiner definierten Lage im Bohrloch (inkl. Wandabstand der Rohre zum Bohrloch). Dadurch werden der thermische Kurzschluss, der Einfluss der Rohrwanddicke, die Eigenschaften des Verfüllbaustoffs und bei Bedarf die Grundwasserströmung berücksichtigt. Ergebnis ist ein exakter, zeitlich hochaufgelöster Betriebsverlauf, der sich auch in Referenzanlagen bestätigt hat.

Mittels ModThermWg und ModGeo3D wurde eine Simulationskampagne durchgeführt. Dabei entstandene Kennfelder stehen intern für eine softwaregestützte Schnellauslegung für Einzelsonden und Sondenfelder bereit. Ausgelegt wird der Bedarf an Ringrohrsonden und Doppel-U-Rohrsonden in Anzahl und Länge im Vergleich. Für größere Sondenfelder ist eine anschließende genauere Auslegung unerlässlich. Es stehen mit der Schnellauslegung aber bereits gute Anhaltspunkte bereit. Eine Onlineversion ist in Arbeit.

DOI: 10.53196/gtj-2023.1

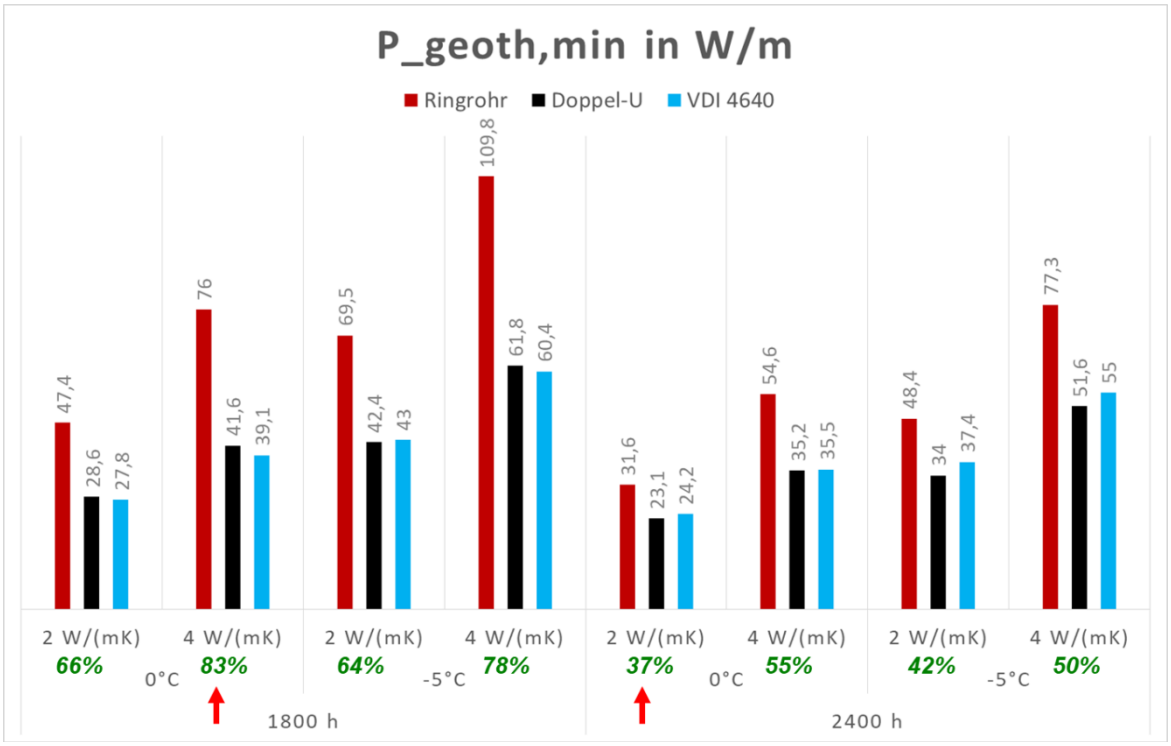

Abbildung 3: Spezifische Leistung für Ringrohrsonde, Doppel-U-Rohrsonde und VDI 4640 über Betriebsstunden der Wärmepumpe je Jahr (h), VL-Temperatur (°C) und Bodenwärmeleitfähigkeit (W/(mK))

VALIDIERUNG VON MODTHERMWG MIT VDI 4640

Zur Überprüfung der Simulationsergebnisse ist ein Vergleich mit dem aktuellen Stand des Wissens und der Technik zweckmäßig. So wurden die Simulationen für die Ringrohrsonde (10 á 16x1,5, 40x3,7) und für die Doppel-U-Rohrsonde (32x2,9) streng nach dem Schema der VDI-Richtlinie 4640 Blatt 2 Seite 104 ff. durchgeführt. Es zeigt sich in Abbildung 3, dass die Werte aus der VDI 4640 (rechter Balken der Dreiergruppe) mit den simulierten Werten aus ModThermWg für die Doppel-U-Rohrsonde (mittlerer Balken) sehr gut übereinstimmen. Die Werte der VDI 4640 basieren auf Berechnungen mit EED für Doppel-U-Rohrsonden mit einer Wärmeleitfähigkeit des Verfüllmaterials von 0,8 W/(mK). Damit ist der erste Schritt der Validierung erfolgreich abgeschlossen worden.

Für die Ringrohrsonde zeigen sich deutlich höhere spezifische Leistungen als für die Doppel-U-Rohrsonde. Ersichtlich ist, dass die Leistungsfähigkeit der Ringrohrsonde gegenüber der Doppel-U-Rohrsonde bei geringeren Jahresbetriebsstunden und höheren Bodenwärmeleitfähigkeiten auch relativ steigt.

Der Nachweis für die hohe Leistungsfähigkeit der Ringrohrsonde wird im Folgepunkt gezeigt.

DOI: 10.53196/gtj-2023.1

VERGLEICH VERSCHIEDENER ERDWÄRMESONDEN (EWS) AN EINER REFERENZANLAGE

Zur Bestätigung der hohen Leistungsfähigkeit der Ringrohrsonde nach den Simulationsdaten wurde ein reales Kundenprojekt mit verschiedenen EWS realisiert und mit zusätzlicher Messtechnik (VL-, RL-Temperaturfühler, Volumenstrommesser) ausgestattet. Anonymisiert wird das aus 3 EWS bestehende Sondenfeld als Anlage E geführt. Es besteht aus einer RRS mit Verfüllschlauch (RR1), einer RRS ohne Verfüllschlauch (RR2) und einer Doppel-U-Rohrsonde (US3).

Sie sind im Abstand von 7 m zueinander abgeteuft (Tiefe 80 m) und an die gleiche Wärmepumpe angeschlossen. Die Volumenströme (18 l/min.) und die VL-Temperaturen (Injektionstemperaturen) aus der Wärmepumpe sind gleich groß. Das ermöglicht einen direkten Vergleich der Leistungsfähigkeit der drei EWS.

Das Verfüllmaterial hat für alle drei EWS den Wärmeleitwert von 0,8 W/(mK). Die Position der Doppel-U-Rohrsonden im Bohrloch ist allerdings zumeist willkürlich, was stellenweise auch Wandanlage ausdrücklich einschließt. Das vermindert den thermischen Bohrlochwiderstand.

Der Verlauf der Messdaten als Tagesmittelwerte ist in Abbildung 4 gezeigt. Bei einer Bodenwärmeleitfähigkeit von ca. 1,8 W/(mK) ergibt sich für die Ringrohrsonde (RR1) eine um 37 % höhere Leistungsfähigkeit gegenüber der Doppel-U-Rohrsonde (US3) bei gleicher Zirkulationsrate. Wie aus Abbildung 4 ersichtlich, liegt die Rücklauftemperatur der RR1 um ca. 0,4 K über der von US3, so dass eine Erhöhung der Zirkulationsrate in RR1 um 6 l/min. auf 24 l/min. zu einer weiteren Leistungserhöhung um etwa 8 % geführt hätte. Die Volllastnutzungsdauer der Anlage E liegt bei ca. 2200 Jahresbetriebsstunden.

Die Ringrohrsonde ohne Verfüllschlauch (RR2) ist nur minimal besser als die Doppel-U-Rohrsonde – eine Folge der willkürlichen Rohranordnung gegenüber der RR1.

An der passiven Kühlung nehmen RR2 und US3 praktisch kaum Teil. Fast die komplette Kühlung übernimmt die mit dem Erdreich optimal verbundene Ringrohrsonde (RR1).

In einer dritten Stufe der Validierung (Abbildung 5) werden die gemessenen VL-

DOI: 10.53196/gtj-2023.1

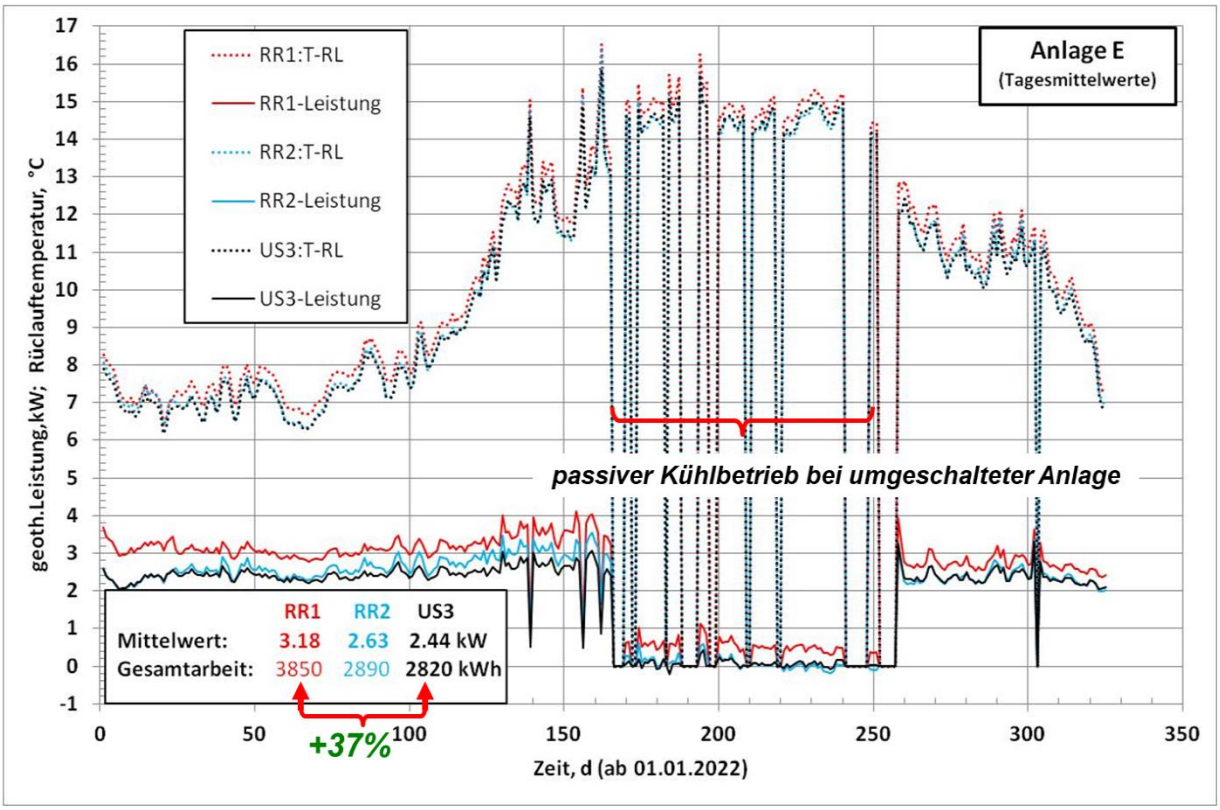

Abbildung 4: Jahresverlauf in Tagesmittelwerten für die Ringrohrsonde mit Verfüllschlauch (RR1), die RRS ohne Verfüllschlauch (RR2) und Doppel-U-Rohrsonde (US3) für die Referenzanlage E

Temperaturen der EWS als Eingangsparameter für die Simulation in ModThermWg eingesetzt. Simulationsverlauf und Messpunkte ähneln sich sehr. Die mittlere quadratische Abweichung der simulierten von der gemessenen Wärmeleistung für die Doppel-U-Rohrsonde liegt bei 16,5 % (bezogen auf die mittlere gemessene Wärmeleistung), die für die Ringrohrsonde bei 21,7 %. Die Abweichungen bewegen sich in einem akzeptablen Korridor. Messungen und Simulation zeigen für die Ringrohrsonde auch hier wieder die höhere Leistungsfähigkeit.

Auch die Messungen der zweiten und dritten Stufe der Validierung zeigen die hohe

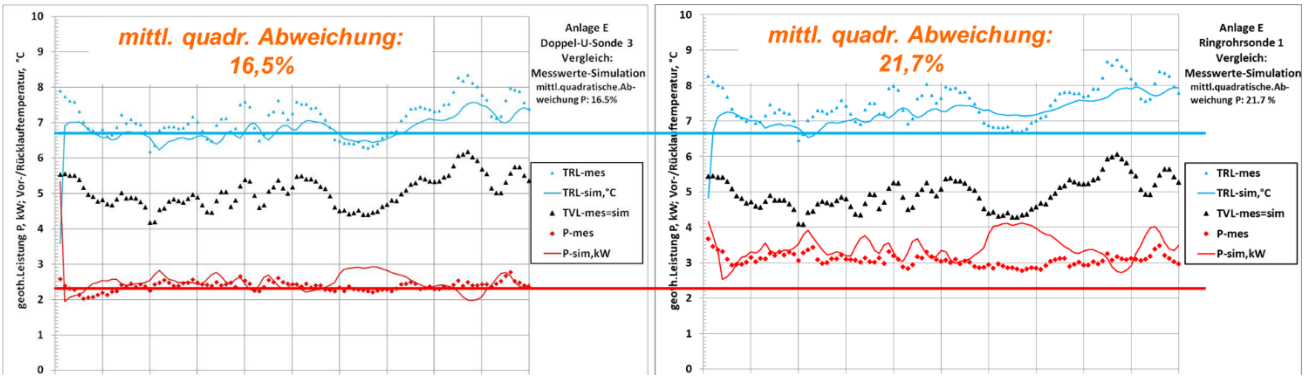

Abbildung 5: Doppel-U-Rohrsonde (US3) und Ringrohrsonde (RR!) im direkten Vergleich gemäß Messungen und Simulation

DOI: 10.53196/gtj-2023.1

Leistungsfähigkeit der Ringrohrsonde und des ModX-Softwarepakets.

ZUSAMMENFASSUNG

Die als Wärmewende bezeichnete Umstellung der Gebäudeheizung und -klimatisierung auf CO_2-freie bzw. -arme Verfahren lässt sich nur unter Einsatz von Wärmepumpen erreichen.

Die von Erdwärmesonden versorgte Anlage hat dabei die beste energetische Effizienz. Gerade hier gibt es in Errichtung und Betrieb großes Einsparpotenzial. Die neuartige Ringrohrsonde hebt dieses Einsparpotenzial. Einsparungen von mindesten 35 % an Bohrmetern oder an Anzahl Bohrungen vermindern die erforderlichen Aufwendungen für

- die Bohrungen und den dadurch verbundenen Energie- und Materialaufwand,
- den Verbrauch für das Sondenmaterial und die Sole,
- bei Sondenfeldern (ab 2 EWS) auch den obertägigen Verrohrungsaufwand und
- den elektrischen Stromverbrauch der Soleumwälzpumpe durch kürzere Strömungswege.

In Summe ergeben sich dadurch Kosten-einsparungen in Anschaffung und Betrieb.

In Kombination mit der erforderlichen Geschwindigkeit, in der die Energiewende vorangehen soll, muss auch die Kapazität an Heizungsbauern und Bohrunternehmen für die Errichtung von neuen Heizungs- und Erdwärmesondenanlagen berücksichtigt werden. Prinzipiell könnten bei 35 % Einsparung an Bohrmetern auch deutlich mehr Geothermieanlagen errichtet werden.

Die Ringrohrsonde hat das Potenzial die Energiewende weiter zu beschleunigen, erheblich Ressourcen einzusparen und den CO_2-Fußabdruck deutlich zu senken.

LITERATUR

[1] Häfner, F., Wagner, R.M., Meusel, L.: Bau und Berechnung von Erdwärmeanlagen. Springer Vieweg, 2015

SCHLÜSSELWÖRTER

Ringrohrsonde, Geothermie, Energiewende, Simulation, Erdwärmesonde, Doppel-U-Rohrsonde, Sondenfelder

DOI: 10.53196/gtj-2023.1

Modern seismic reprocessing to cope the demands of geothermal projects

Claudia Schimschal, Thomas Fieseler, Gerald Klein, Eliakim Schünemann

TEEC GmbH

30916 Isernhagen

Germany

ABSTRACT

While seismic imaging is standard in the exploration of oil and gas fields, its significance is growing as the basis for success of geothermal projects. Standard seismic processing strategies work for areas with simple geology, but do not lead to satisfactory results in complex geologic settings. As geothermal projects regularly face such complexity (e.g. the fault systems of the Rhine Graben), the applied standard and often outdated seismic processing techniques do not provide sufficient subsurface imaging. Experience from numerous projects in highly complex geologic settings shows that five key steps are crucial to overcome these difficulties: 1. Near surface velocity model and basic statics solution, 2. surface wave suppression, 3. increase in signal-to-noise ratio and data regularization, 4. stacking/migration velocities and residual statics and 5. sophisticated imaging e.g. the Reverse Time Migration and interval velocity model. In this paper, we will present examples and further information on these key steps.

Keywords: Seismic Processing, Imaging of Faults, Reverse Time Migration, Full Waveform Inversion

DOI: 10.53196/gtj-2023.1

INTRODUCTION

To implement successful geothermal projects, a careful drill path planning is mandatory. Drill path, drill location and target depth are planned based on a seismic image. Thus, the success of the entire geothermal project depends on the accuracy of this seismic image [1, 2]. Therefore, seismic is a small but very crucial step in the success of a geothermal project. The complexity of geologic settings, (e.g. steep dips, faults) and problems due to the proximity to civilization (strong ambient noise, limited frequency content, data gaps) of various geothermal locations require enhanced processing strategies for a convincing and veritable image on which the geologic model is based [3, 4, 5, 6]. Insufficiencies resulting from outdated or inappropriate processing strategies include the loss of amplitude conservation, resolution, reflection continuity and frequency content. In addition, a poor resolution of near-surface velocity variations worsens the image significantly even in deeper parts [7]. Due to smooth travel time requirements, ray-based depth migration techniques such as Kirchhoff or Beam are inadequate for the complex velocity models involved in these areas. This may lead to a horizontally shifted location of faults in the range of tens to hundreds of meters [8]. Considering drill path and target depth planning, these are uncertainties that threaten the success of the entire geothermal project. All these shortcomings cause problems and costs that enhanced seismic data processing could avoid [1]. Experience from projects from the oil and gas industry, nuclear waste deposits and geothermal projects led to the development of advanced technologies, methods and strategies, which will be described in more detail in this paper.

METHOD

1. Near surface velocity model and basic statics solution

The first step to successful imaging is the near surface velocity model and the associated basic statics solution. Directly below surface, small geologic structures like infills or quaternary bodies and outcropping or eroded layers can cause a higher variety of velocities compared to deeper laying layers. When the seismic wave travels through these small structures, a misfit in travel time results, which is even twice in the data as the seismic wave travels downwards and upwards through these anomalous velocity zones. The basic statics corrections are meant to remove

DOI: 10.53196/gtj-2023.1

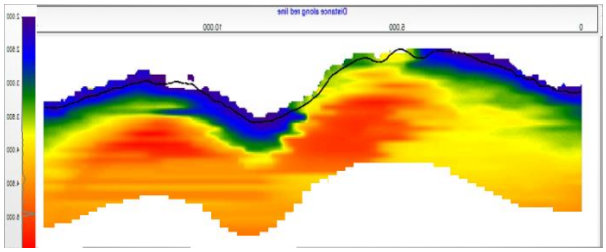

Figure 1: Velocity model from the first break tomography calculated with constant node spacing.

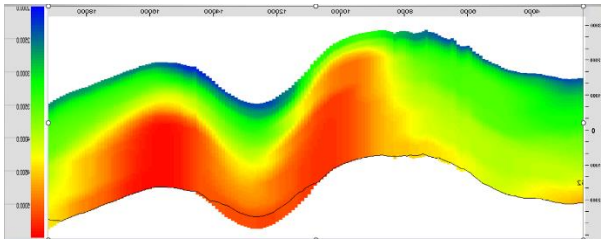

Figure 2: Velocity model from the first break tomography calculated with variable node spacing.

the impact of vertical and lateral variations in the near surface velocity and compensate for the difference in seismic travel time caused by such variations. In settings with topography and/or highly variable subsurface velocities, standard refraction or elevation statics fail to provide accurate results as they suggest structures in time domain which are due to velocity variations. Here, tomographic approaches are key to remove shallow subsurface velocity effects. A standard first break tomography is based on a regular grid of nodes which are then updated by an inversion process based on first break pick times. A better approach is a variable node spacing tomography. Here, the grid for calculation starts at topography and has smaller distances between nodes close to the surface and a wider spacing with increasing depth. This way, small-scale velocity changes close to the surface can be included in contrast to a regular constant grid size. The result is a high-resolution velocity model in depth domain below surface. Figure 1 shows the result of a first break tomography calculated with a constant node spacing of 50 m. Figure 2 displays the tomography result for the same section calculated with a variable node spacing of 10 m at the surface increasing to 100 m at the bottom of the model in ~2 km depth. Its lateral node spacing is constant with 50 m. While the velocity model with the standard approach implies blocky structures, the variable node spacing tomography results in a smoother velocity field. Both models pick up the deeper high velocity zone correctly. In the shallow part, the velocity model from variable node spacing tomography is much more detailed and shows less thickness of the low velocity zone. The tomography result is used to calculate a static solution. Figure 3 and Figure 4 show the effects of the static solution on the seismic stack. Even for the deeper part the visibility and continuity of reflectors are improved with the static solution from the variable node spacing tomography in Figure 4 compared to the standard solution in Figure 3.

DOI: 10.53196/gtj-2023.1

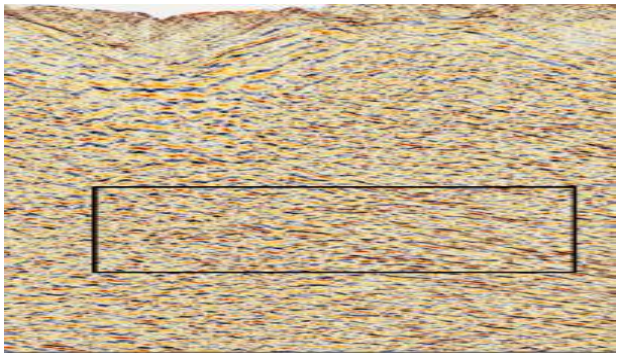

Figure 3: Seismic stack with static solution from a constant node spacing tomography.

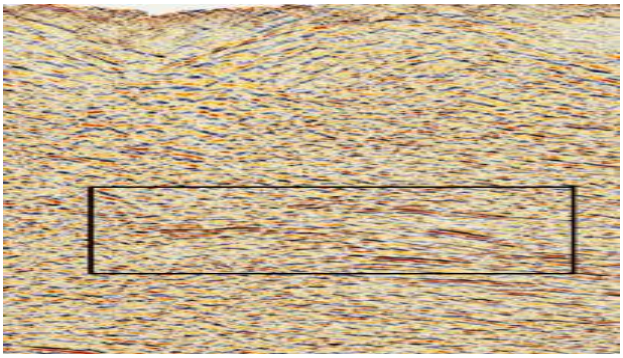

Figure 4: Seismic stack with static solution from a variable node spacing tomography.

2. Noise model and adaptive subtraction

One aim of processing is to "denoise" the seismic data, which means to reduce the noise and thereby amplify the primary signal. The surface wave exhibits high amplitude levels and overlays the primary reflection signal in the shot cone completely (Figure 5). Therefore, its suppression is an important part of the denoise process. To eliminate this noise, the surface wave can be modelled and subtracted from the input data. Here, a simple subtraction of the model delivers reasonable results at a first glance: Figure 5 shows the input shot gather with the noise of the surface wave, the shot gather after standard subtraction is plotted in Figure and in Figure after adaptive subtraction. With both methods the noise in the shot cone is eliminated and the results look very similar. Nevertheless, if we look at the frequency spectrum in Figure 6 the difference between both methods is clearly visible. A significant portion of the intensity of low frequencies are missing after standard subtraction. These are preserved with the adaptive subtraction. Here, the surface wave model will be adapted to the input data regarding frequency content, amplitude, and phase prior to subtraction. Hence, the low frequency content is preserved and enables broadband processing. This is also of great importance for later steps like the Full Waveform Inversion (FWI), which needs low frequencies for a stable inversion. Figure 7 and Figure 8 show the difference between the result after subtraction and the input data. One can observe that standard subtraction (Figure 7) also removes primary energy, which is reduced with adaptive subtraction (Figure 8).

DOI: 10.53196/gtj-2023.1

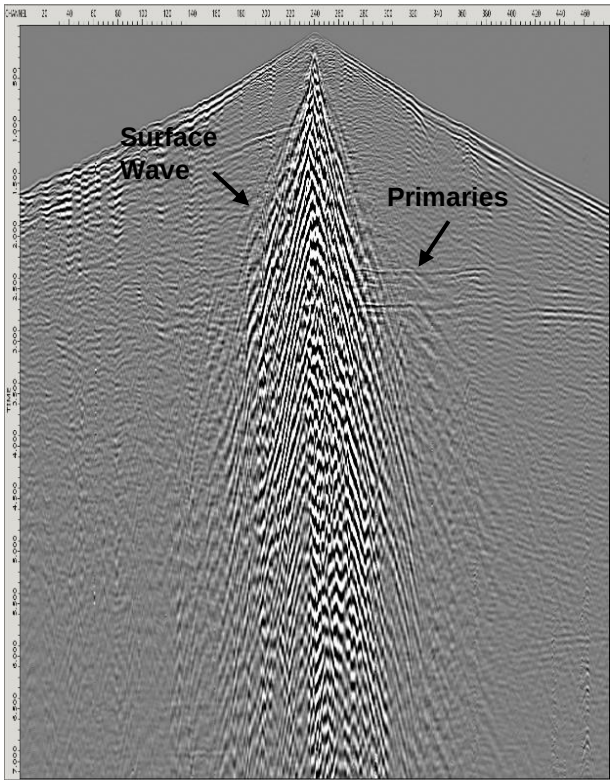

Figure 5: Shot gather before surface wave subtraction. Its noise is visible in the shot cone.

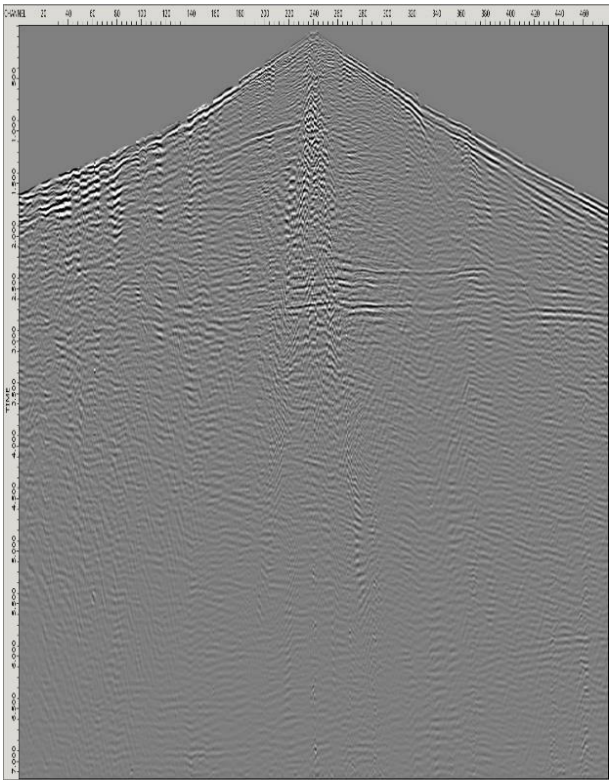

Figure 7: Shot gather after adaptive subtraction of the noise model.

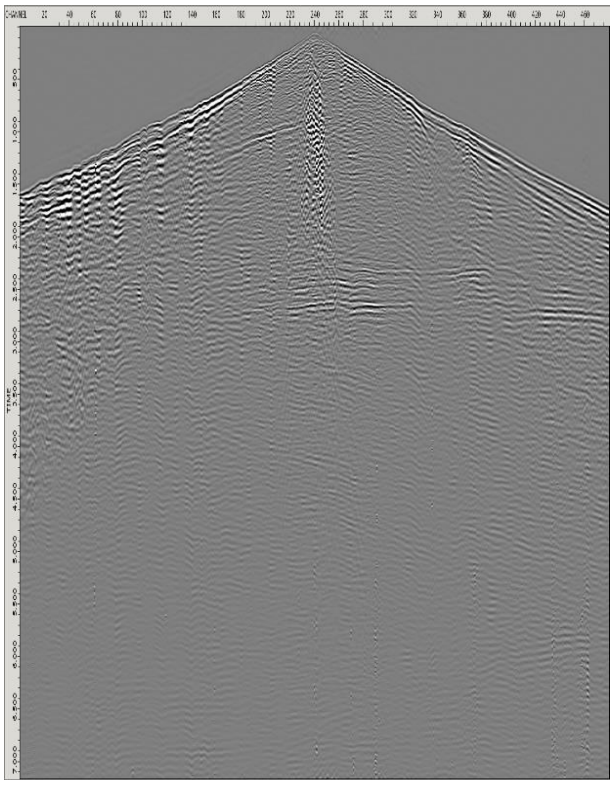

Figure 6: Shot gather after standard subtraction.

Figure 6: Spectrum after standard subtraction (red) and adaptive subtraction (green, dashed). Note that part of the low frequency content is missing after standard subtraction.

DOI: 10.53196/gtj-2023.1

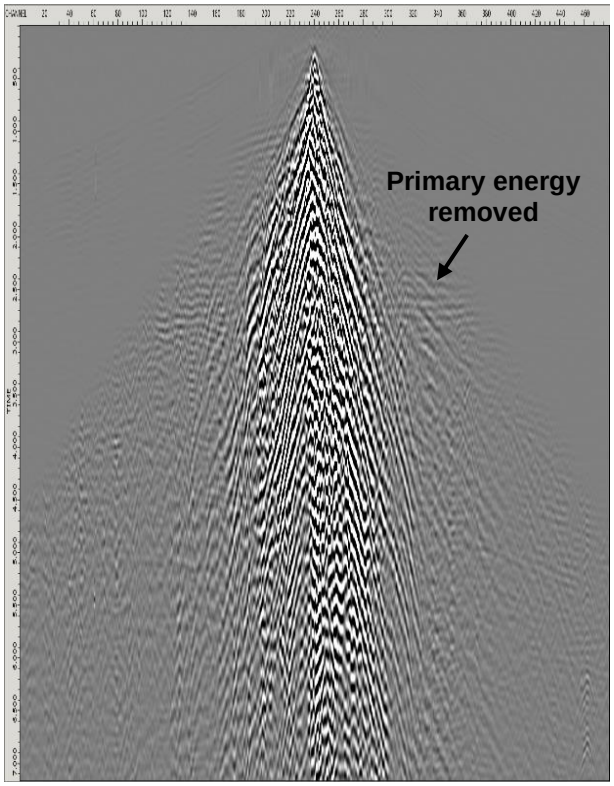

Figure 7: Difference between input data and result after standard subtraction.

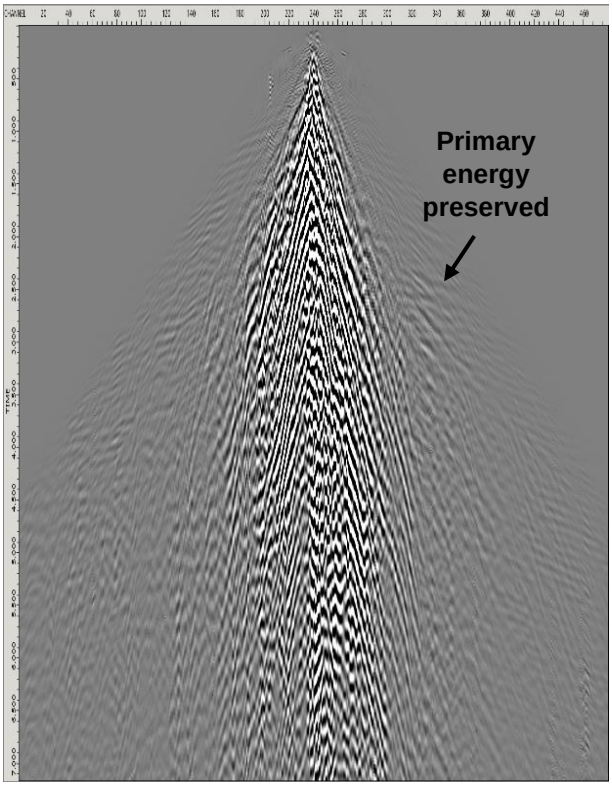

Figure 8: Difference between input data and result after adaptive subtraction.

3. Common Reflection Surface (CRS)

The first approaches to stack a seismic section included only the common mid-point (CMP) location. The underlaying normal moveout (NMO) model assumed just flat layers in the subsurface [9]. This model was extended to include the dip component by dip moveout (DMO) processing [10]. In addition to dip and depth, CRS analyses the curvature of subsurface reflection elements [11]. These wavefront attributes are even accurate for complex media and useable for applications such as data regularization, interpolation, or diffraction processing [12]. The CRS stacking operator is not limited by a surface bin cell anymore but includes the energy from the entire Fresnel zone. Hence, if a reflector element is illuminated by the seismic acquisition, CRS processing will probably be able to collect such energy [11]. The CRS algorithm improves the data quality significantly, especially in areas with a low signal-to-noise ratio [13]. Furthermore, CRS can be used for data regularization, which influences the migration result considerably. Irregularities in receiver/shot locations result in an irregular fold of coverage and data gaps, which likely lead to migration artefacts. CRS processing along with 5D interpolation are

DOI: 10.53196/gtj-2023.1

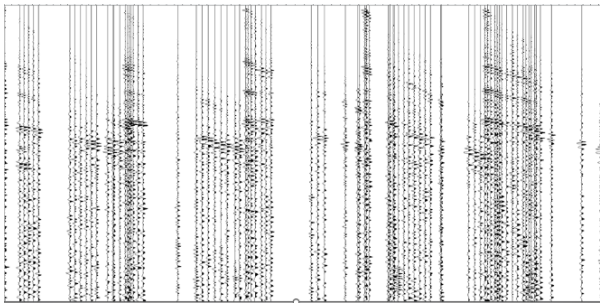

Figure 9: CMP gather before CRS.

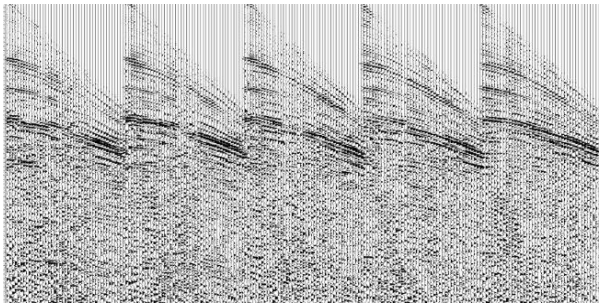

Figure 13: With CRS regularized Gather.

modern regularization techniques with CRS even working in areas where 5D often fails such as low signal-to-noise ratio, low fold of coverage and steep dips. An irregular acquisition layout is a common problem for geothermal projects. These projects are typically close to civilization. Infrastructure, buildings and no permit zones, e.g. nature conservation areas, prevent a regular acquisition layout. Figure 9 shows CMP gather with an irregular trace spacing and missing traces in many offset classes. After CRS prestack data regularization, the bin gathers are properly filled and show an improved signal-to-noise ratio (Figure 13). The irregularities without CRS will affect the prestack time migration significantly and lead to a poor seismic image (Figure 12). In contrast, CRS improves the prestack time migration especially for areas with data gaps (Figure 10). With greater depth, reflectors become visible that are overlain by noise without CRS.

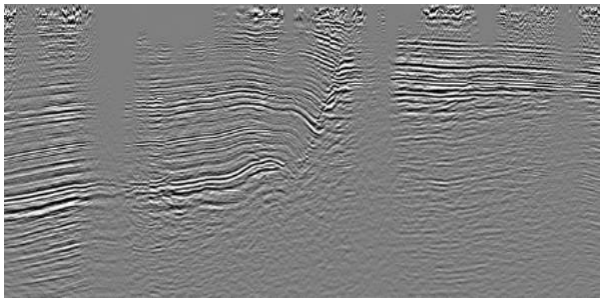

Figure 12: Prestack Time Migration result without CRS.

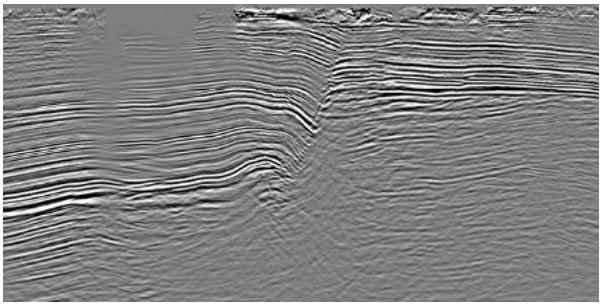

Figure 10: Prestack time migration result after CRS application.

DOI: 10.53196/gtj-2023.1

4. Stacking velocity analysis, residual statics, and migration velocity analysis

Stacking velocity analysis, residual statics, and migration velocity analysis benefit from all previously described steps with a proper basic static, enhanced denoising and an improved signal-to-noise ratio. In Figure 11 an uncorrected CMP gather (left), the semblance (middle) and the normal moveout (NMO) corrected CMP gather (right) are displayed. Reflections are hyperbolic in the uncorrected gather. They become flat, when the correct NMO velocity is applied. For the correct NMO, the semblance is maximum because the seismic wavelet of NMO corrected adjacent traces is similar (have their peaks/troughs at the same time). Due to high noise levels, the semblance of the CMP gathers shows no clear trend. In Figure 12 the same gather is displayed with CRS processing applied. Here the CRS gather shows a much better data quality and allows for a more reliable identification of reflection signal. Hence, the semblance is better focused and a clear velocity trend becomes visible. An additional step to improve the stacking velocity are constant velocity stacks. The entire section is stacked multiple times with one constant velocity (e.g., with velocities from 1,5 to 5 km/s with an increment of 0,1 km/s). This provides a quality control as all real structures visible in these stacks must be present in the final result. Migration velocity analysis in time domain can be performed likewise. The velocity can be picked with the uncorrected and corrected Common Image Gather and their semblance as well as with constant velocity migrations. For the migration velocity in time domain also percentage velocity variations (of the stacking or preliminary migration velocities) can be calculated. The percentages for which the Common Image Gather show flat events are picked and multiplied with the input velocity field.

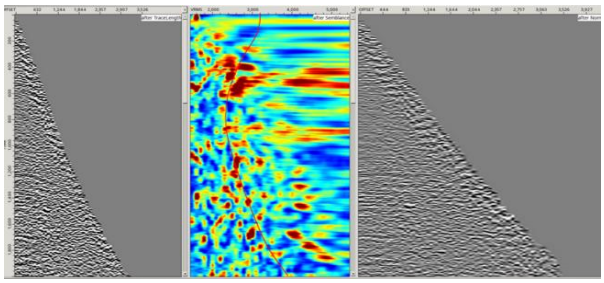

Figure 11: Uncorrected CMP gather (left), semblance (middle) and NMO corrected gather (right).

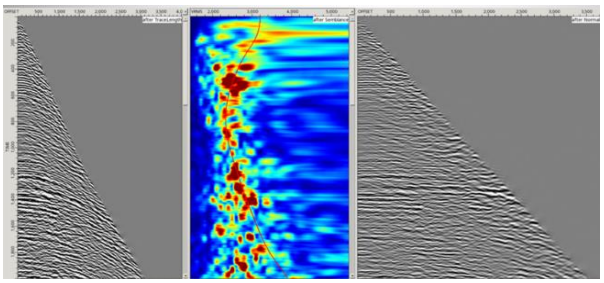

Figure 12: Uncorrected CRS gather (left), semblance (middle) and NMO corrected CRS gather (right).

DOI: 10.53196/gtj-2023.1

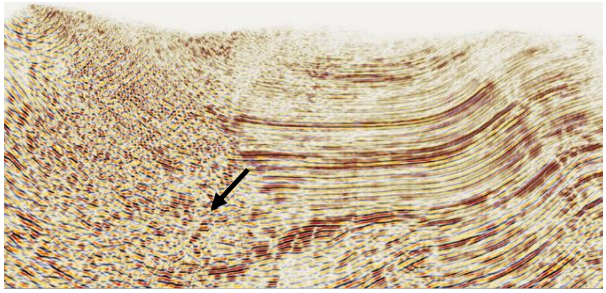

Figure 13: Result of Kirchhoff Depth Migration with CRS applied.

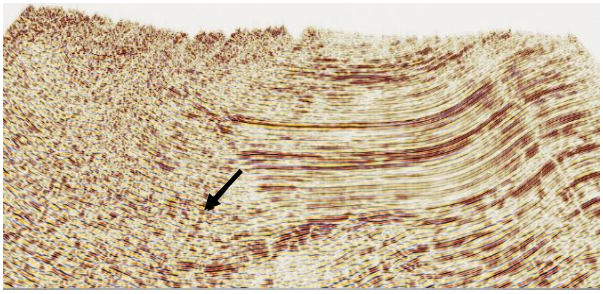

Figure 14: Result of the RTM with CRS applied.

5. Reverse Time Migration (RTM) and Full Waveform Inversion (FWI)

Correct positioning of geologic structures is mandatory in seismic depth imaging. As ray-based depth migration techniques, which are standard in processing, fail to solve travel times correctly for complex velocity models, the usage of the RTM is favored. By solving the acoustic wave equation, the RTM realistically simulates the propagation of waves through the subsurface. This way, the algorithm can account for any complexity in the velocity model [8]. The seismic image calculated with a Kirchhoff Depth Migration (Figure 13) can be compared to the result of the RTM in Figure 14. For the sedimentary structures both migration algorithms provide reasonable results. But the RTM yields a much clearer image for the complex geology on the left side of the section. The data continuity and visibility of reflectors is increased significantly in the questionable area. Moreover, the fault (marked with an arrow in Figure 13 and Figure 14) has moved by about 200 m to its actual location. The correct positioning of faults is of great importance e.g. for the planning of the drill site and drill path.

In the previous section about the near surface velocity model and the basic statics solution, the importance of the correct near surface velocities was emphasized. As only few traces cover the upper ~150 ms (compare Figure 12), information about the velocity structures directly below the surface can hardly be retrieved by analyzing the gather during the standard velocity analysis. In addition to the velocity model from the first break tomography that is used for the basic static solution, the FWI is able to enhance the near surface velocity model significantly. The FWI is an iterative approach to find the best sub-surface model by minimizing the difference between the observed waveform and a calculated synthetic waveform in amplitude and phase in a dedicated frequency band. For

DOI: 10.53196/gtj-2023.1

a successful FWI calculation, the simulated waveform of the starting model needs to be less than half a wavelength apart from the wavelength of the observed data. Otherwise, artefacts are introduced into the velocity model by cycle-skipping, which means matching two different phases that do not belong to each other. To overcome the cycle skipping problem, the FWI requires low frequency data content. This way, the size of the wavelength is increased and the algorithm is stabilized [14]. Furthermore, with the velocity model derived from the first break tomography an initial model is available which is already close to the real sub-surface velocities. Figure 15 and Figure 16 illustrate the effect of the enhanced velocity model from the FWI on the seismic image. In the image calculated with the velocities without FWI (Figure 15) the velocities increase with depth. There are no clear geologic structures visible except for the dipping structure in the central part of the section. The velocities from the FWI follow the geologic structures and are higher than in the initial velocity model for the upper part of the section (Figure 16). By including the FWI velocities, a basin and faults are revealed that were not visible before.

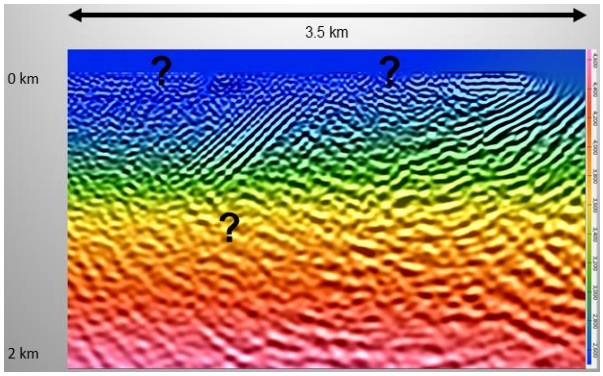

Figure 15: Depth migration result calculated with the velocity model from the tomography, which is displayed in the background.

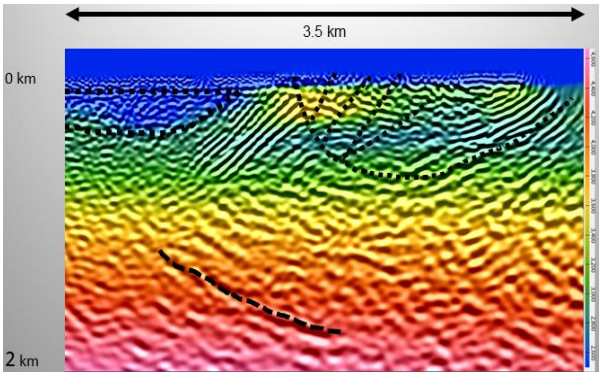

Figure 16: Depth migration result calculated with the velocity model from the FWI, which is displayed in the background.

CONCLUSION

Modern seismic reprocessing methods enable to solve difficulties that threaten the success of an entire geothermal project. Complex geologic settings with steep dips and faults can be imaged correctly by using CRS in combination with an RTM as a modern migration algorithm. These methods further profit from the correct near surface velocities calculated with a variable node spacing tomography in combination with an FWI.

DOI: 10.53196/gtj-2023.1

Typical problems of geothermal projects result from the proximity to civilization. These include strong ambient noise that can be reduced by enhanced denoising and CRS. Data gaps can be filled with CRS. The frequency content is preserved by methods like an adaptive subtraction that enables broadband processing. The resolution and reflection continuity are improved by all presented processing steps. Furthermore, the methods better preserve amplitudes enabling amplitude analysis for reservoir characterization. All these processing steps result in an enhanced seismic image that is crucial for the success of a geothermal project.

ACKNOWLEDGEMENTS

Anja Kosin is thanked for her efforts to improve this manuscript. Hocol, Ecopetrol and EBN are thanked for their permission to show the data. Software from TEECware was used for processing. The FWI development was supported in the WAVE research project (Grant No. 01IH15004) funded by the Bundesministerium für Bildung und Forschung (BMBF) and in the FWIGREM research project (Grant No. 03SX589B) funded by the Bundesministerium für Wirtschaft und Klimaschutz (BMWK). The anonymous reviewer is thanked for the constructive feedback.

REFERENCES

[1] M. Casini, S. Ciuffi, A. Fiordelisi, A. Mazzotti, E. Stucchi (2010): “Results of a 3D seismic survey at the Travale (Italy) test site”, Geothermics, Volume 39, Issue 1.

[2] N. Salaun, H. Toubiana, J.-B. Mitschler, G. Gigou, X. Carriere, V. Maurer, A. Richard (2020): “High-resolution 3D seismic imaging and refined velocity model building improve the image of a deep geothermal reservoir in the Upper Rhine Graben”, The Leading Edge 2020.

[3] S. Chopra, K. J. Marfurt (2005): "Seismic attributes - A historical perspective", GEOPHYSICS 70.

[4] C. Schmelzbach, S. Greenhalgh, F. Reiser, J.-F. Girard, F. Bretaudeau, L. Capar, A. Bitri, (2016): "Advanced seismic processing/imaging techniques and their potential for geothermal exploration", Interpretation 4: SR1-SR18.

[5] D. L. Siler, J. E. Faulds, B. Mayhew, D. D. McNamara (2016): “Analysis of the favorability for geothermal fluid flow in 3D: Astor Pass geothermal prospect, Great Basin, northwestern Nevada, USA”, Geothermics, Volume 60.

[6] Q. Yasin, A. Gholami, M. Majdański, B. Liu, N. Golsanami (2023): “Seismic characterization of geologically complex geothermal reservoirs

by combining structure-oriented filtering and attributes analysis", Geothermics, Volume 112.

[7] I. Jones (2012): "Incorporating Near-Surface Velocity Anomalies in Pre-Stack Depth Migration Models", First Break 30.

[8] G. Gierse, E. Schuenemann, E. Tessmer, R. Ballesteros and H. Salazar (2011): "Depth imaging using CRS shot gathers in reverse time migration", SEG Technical Program Expanded Abstracts: 3300-3304.

[9] W. Mayne (1962): "Common reflection point horizontal stacking techniques", Geophysics. 27, 927-938.

[10] D. Hale (1991): "Dip Moveout Processing", Society of Exploration Geophysicists.

[11] J. Mann, R. Jaeger, T. Mueller, G Hoecht, and P. Hubral (1999): "Common-reflection surface stack - A real data example", Journal of Applied Geophysics, 42, No. 3, 4, 283–300.

[12] D. Gajewski (2019): "Wavefront attributes - A tool for processing, imaging, and model building", SEG Honorary Lecture Program 2019.

[13] G. Eisenberg-Klein, J. Pruessmann, G. Gierse, H. Trappe (2008): "Noise reduction in 2D and 3D seismic imaging by the CRS method", The Leading Edge (2008) 27 (2): 258–265.

[14] G. Eisenberg-Klein, E. Verschuur, S. Qu, E. Schuenemann, (2019): "JMI-FWI: Cascading Workflow Using Joint Migration Inversion (JMI) and Full Waveform Inversion (FWI)", European Association of Geoscientists & Engineers, Second EAGE/PESGB Workshop on Velocities, Apr 2019, Volume 2019.

DOI: 10.53196/gtj-2023.1

Multi-Objective Parameter Dependencies in the Design of Ground Source Heat Pump Systems

Sebastian Weck-Ponten, Jérôme Frisch, Christoph van Treeck

Institute of Energy Efficiency and Sustainable Building E3D, RWTH Aachen University

ABSTRACT

This paper investigates the parameter dependencies in the design of ground source heat pump systems (GSHPS) for heating and domestic hot water purposes. Based on parameter studies using the system configurator GeoWPSys+Web, the system interrelationships in the design of GSHPS are analyzed with regard to technical, energetic, economic and ecological evaluation parameters. The cost-effectiveness and the ecological evaluation parameters are highly dependent on the building's energy demand and on the seasonal coefficient of performance (SCOP). Economic savings of a GSHPS compared to a gas condensing boiler (GCB) mainly depends on the investment costs as well as on the gas and electricity prices and their annual increases. In addition to economic and technical variation options, GeoWPSys+Web can also map influences on CO_2 emissions of the GSHPS. For example, the CO_2 emissions of the monovalent reference case can be more than halved over a period of 20 years with an increased feed-in of renewable electricity into the German electricity mix and a resulting annual reduction of the CO_2 equivalent for electricity by 10%.

Keywords: Planning dependencies, shallow geothermal energy, ground source heat pump systems, system configuration, system configurator, system design, heat pump

INTRODUCTION

GSHPS can play a central role in boosting the heat transition and the decarbonization of the heating sector. However, the expansion of

DOI: 10.53196/gtj-2023.1

shallow geothermal systems is stagnating due to an acute shortage of craftsmen and drilling companies, high investment costs, and a complex planning and approval process. In the planning of GSHPS, different methods and tools are used, various planning trades are involved and a variety of design parameters exists that influence each other [1].

Many studies on GSHPS examine an optimal design of the geothermal source system (GSS) in terms of economics (see [2], [3], [4], [5], [6], [7]) or the heat pump efficiency (see [3],[8],[9], [10], [11], [12]) or other evaluation parameters (see [4], [6]). These studies usually focus on subsurface properties, the depth of borehole heat exchangers (BHE), their geometrical dimensions as well as the geometrical layout of BHE fields. Some of them ([3], [8], [13], [7]) also consider groundwater flows.

Economic relationships between the design of the heat pump (HP), its operating mode and connected buffer and DHW storage tanks are often not examined. The majority of the considered studies mainly use static profitability calculations (see [2], [3], [4], [6]) such as investment costs. Dynamic methods such as the net present value (NPV) method are rarely used (see [5], [7]). None of the economic analyses of the considered studies account for variations of dynamic economical parameters such as the calculation interest rate and price increase rates.

In addition, holistic analyses that include not only economic parameters but also ecological evaluation parameters such as CO_2 emissions are often not carried out.

The objective of this paper is to examine technical, energetic, economic and ecological parameter dependencies in the design of brine-to-water HPs together with BHE, buffer and DHW storage tanks. This study focuses on the design of the HP system (HP as well as buffer and DHW storage tanks) and its effects on the required BHE length as well as on economics and CO_2 emissions of the entire system.

TECHNICAL SYSTEM RELATIONSHIPS

Figure 1 shows the complex technical system relationships of a GSHPS for heating and DHW purposes. In addition to the subsurface properties, the size of the GSS depends on the energy requirements for heating and DHW as well as on the peak loads extracted from the ground. The peak loads are influenced by the annual building energy demands, the size of buffer and DHW storage tanks, the thermal storage capacity of the building and the efficiency of the HP at the respective operating points. Latter is dependent on the supply

DOI: 10.53196/gtj-2023.1

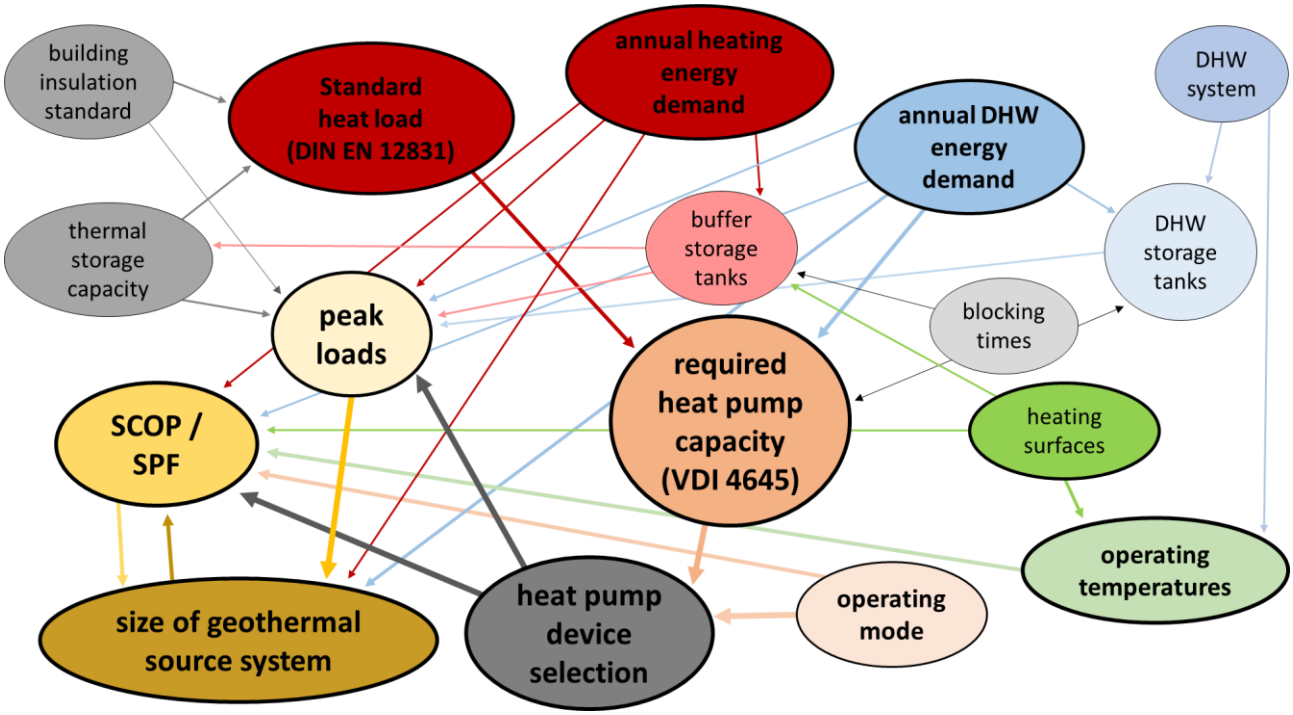

Figure 1: Technical system relationships in the design process of a GSHPS for heating and DHW purposes (based on [1])

temperatures for heating and DHW, the HP's operating mode and the selected HP device. The supply temperatures depend on the heating surfaces (panel heating or radiators) and on the DHW system.

The HP device has a specific coefficient of performance (COP) and nominal capacity in the design point. Based on the operating mode of the HP and the calculated required HP capacity (RHPC) according to the German guideline VDI 4645, a suitable HP device is selected. In the case of a purely electric operation (in Germany defined as the mono-energetic operating mode), the HP can usually be designed smaller, since an electric heating element covers the peak loads. The proportion of the heating element in the total annual energy consumption has an influence on the seasonal performance factor (SPF; measured value) and on the SCOP (calculated value).

The RHPC is calculated based on the standard building heat load ($\dot{Q}_{H,AP}$), the daily energy demand for DHW ($Q_{DP,ges}$), the hours of a day (d), the sum of blocking times of the HP (t_{SD}) and other energy demands (Q_{misc}), e.g. for heating a swimming pool, according to [14] with the following equation:

$$\mathrm{RHPC} = \frac{d \cdot \dot{Q}_{H,AP} + Q_{DP,ges} + Q_{misc}}{d - \sum t_{SD}} \quad (1)$$

The standard heat load depends, among other things, on the building insulation standard and the thermal storage capacity of the building.

DOI: 10.53196/gtj-2023.1

SYSTEM CONFIGURATION

The system interrelationships highlight the need for tool-based planning aids such as the web-based system configurator GeoWPSys+Web. The first version of the system configurator was based on an Excel-tool described in [15]. The tool has been further developed and implemented as a Web-Frontend. GeoWPSys+Web allows a detailed configuration of brine-to-water HPs as well as buffer and DHW storage tanks based on real manufacturer component data. The HP as a single heat generator (in Germany defined as monovalent operating mode) and hybrid HP systems (in Germany defined as bivalent operating modes) are compared with a GCB.

As a first approach, the total length of the BHE (l_{BHE}) is calculated in GeoWPSys+Web in a simplified way using the HP evaporator capacity ($\dot{Q}_{Eva}$) excessed from the subsurface and the specific BHE heat extraction rate ($\dot{q}_{BHE}$) according to [16]:

$$\mathrm{l}_{BHE} = \frac{\dot{Q}_{Eva}}{\dot{q}_{BHE}} \qquad (2)$$

$\dot{Q}_{Eva}$ is determined depending on the design point, taking into account the temperature levels of the heat source and sink side. $\dot{q}_{BHE}$ is a user input dependent on the soil properties at the given project location. In future, the BHE length will be determined based on simulations using bidirectionally coupled subsurface and HP models.

GeoWPSys+Web uses the NPV method to determine the profitability according to [17] using the following equation:

$$K = -\mathrm{I} + \sum_{t=1}^{t_{end}} z \cdot (1+j)^{t-1} \cdot (i+1)^{-t} \qquad (3)$$

The negative investment costs of each component (I) are added to the sum of the time-dependent (t in years) incoming and outgoing difference payments compared to the reference system (z) (e.g. energy costs for electricity and gas, costs for CO_2 or replacement investments) considering price increases (j) and the calculation interest rate (i). The investment costs include, among others, HP devices, buffer and DHW storage tanks, GCBs, circulation pumps, expansion vessels and a chimney in case of a GCB. The energy costs for electricity and gas result from the final energy demand, the generator efficiencies (SCOP or boiler efficiency) and from the costs for electricity and gas including price increases. The electricity and gas costs take into account basic costs and a variable price depending on the amount of energy.

The calculation of the SCOP according to the German guideline VDI 4650 is fully implemented in GeoWPSys+Web and takes into account the coverage shares of the

DOI: 10.53196/gtj-2023.1

individual heat generators in hybrid operation and the respective DHW share of the final energy demand. Latter results from the useful energy requirement for heating and DHW as well as from heat losses from buffer and DHW storage tanks, heating transfer and distribution losses and the generator efficiencies.

The CO_2 emissions and primary energy demand are calculated based on the final energy demand, the CO_2 equivalents and the primary energy factors for electricity and gas. The CO_2 equivalents and primary energy factors can be adjusted for each year of the observation period. Further information about the economic calculations as well as the CO_2 emissions and primary energy demand calculations is described in [1].

The effects of parameter changes are displayed for all system variants simultaneously and immediately in the web-frontend using diagrams, tables and evaluation parameters. In addition, GeoWPSys+Web gives automated system recommendations and numerous assistance options for the user by calculations running in the background and default values for a maximum number of planning parameters.

GeoWPSys+Web is integrated into a multi-level planning tool consisting of a web-based geoportal including databases, building calculation tools, the open source black-box characteristic curve HP system model ModHPS [18] and subsurface models. This enables a system design combined with GIS-based analyses including semi-automatic data aggregation and the determination of hourly building load curves. In addition, investigations of mutual interactions between neighboring BHE are possible via a bidirectionally coupled HP and subsurface simulation considering groundwater flow. The area of application of the multi-level planning tool ranges from individual buildings to urban districts. More information about the multi-level planning tool is described in [1].

RESULTS

The following parameter studies are performed using GeoWPSys+Web and focus on basic parameter relationships, the economic considerations, the CO_2 emissions and the primary energy requirement. When purchasing discounted heat pump electricity tariffs, electric suppliers may block heat pumps at certain times. Table 1 lists the impact of blocking times of the HP on the RHPC. The parameter f corresponds to the denominator of Equation 1 (see Equation 4). Due to blocking times, the HP has to be designed up to 33% larger.

DOI: 10.53196/gtj-2023.1

$$f = \frac{1}{d - \sum t_{SD}} \qquad (4)$$

Table 1: Influence of the blocking times on the calculation of the RHPC

$\sum t_{SD}$	f	%
0	0.042	0
1	0.043	+4.35
2	0.045	+9.09
3	0.048	+14.29
4	0.050	+20.00
5	0.053	+26.32
6	0.056	+33.33

The choice of a larger HP device affects its evaporator capacity at the design point, i.e. the capacity that needs to be extracted from the subsurface at peak load. Thus, the required size of the GSS also increases with longer blocking times (see Equation 2).

Table 4 in the Appendix lists the boundary conditions of the reference case of the parameter studies. Figure 2 shows the results of GeoWPSys+Web for the reference case.

The energy requirements of the building and the SCOP are crucial variables for economic analyses and ecological considerations. GeoWPSys+Web determines the $SCOP_{HPS}$ of the GSHPS according to [19] which includes the HP, the circulation pump of the GSS and an electrically operated peak load heat generator in a mono-energetic case.

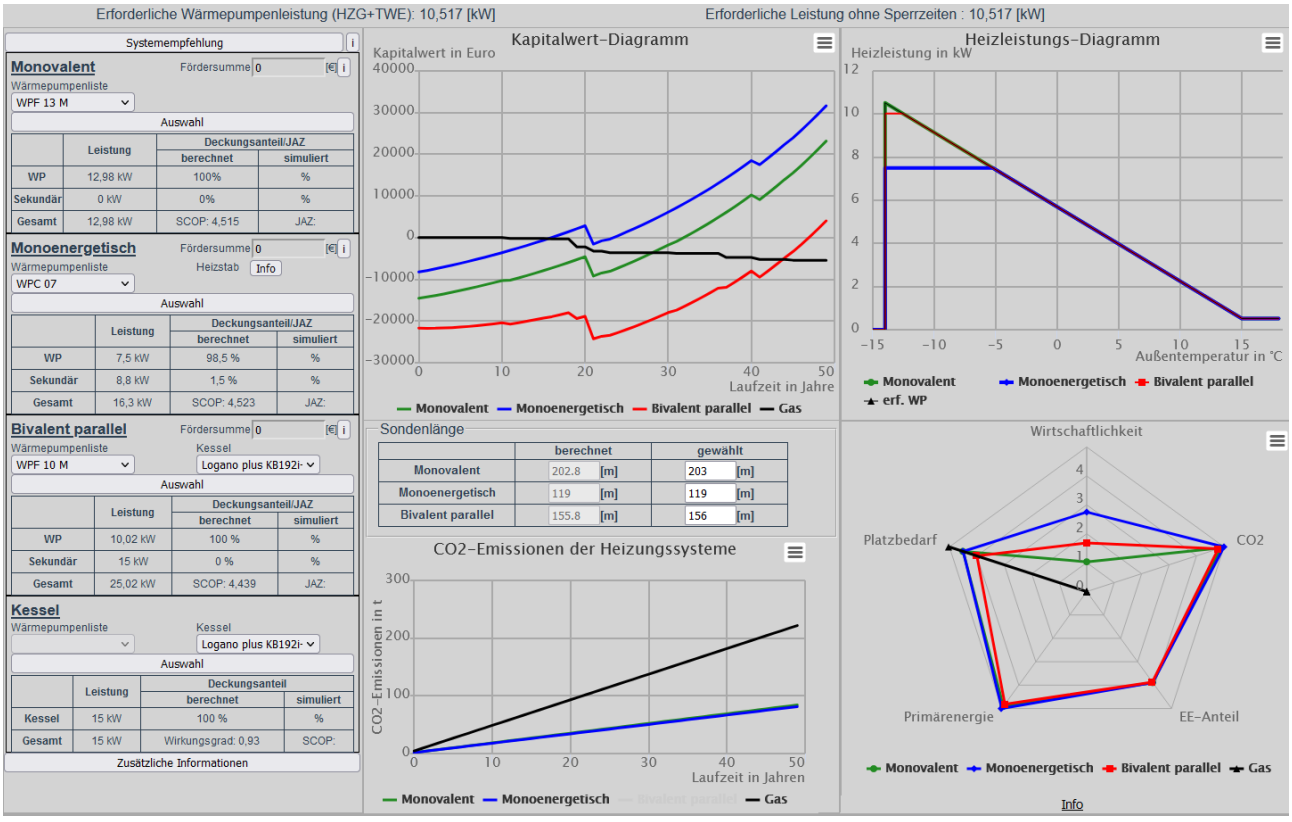

Figure 2: Overview of the results of GeoWPSys+Web of the reference case

DOI: 10.53196/gtj-2023.1

The supply temperatures for heating (T_h) and DHW (T_{DHW}) have a significant influence on the different SCOPs of the monovalent reference case (MRC) (see Equations 5-7, Tables 2-3 and Table 5).

Table 2: $SCOP_h$ as a function of T_h and the percentage deviation of $SCHOP_h$ of the MRC (HP unit WPF 13 M)

T_h	F_ϑ	$SCOP_h$	%
30	1.214	5.361	+5
35	1.157	5.109	0
40	1.099	4.853	-5
45	1.041	4.597	-10
50	0.982	4.336	-15
55	0.921	4.067	-20

Table 3: $SCOP_{DHW}$ as a function of T_{DHW} and the percentage deviation of $SCHOP_{DHW}$ of the MRC (HP unit WPF 13 M)

T_{DHW}	F_1	$SCOP_{DHW}$	%
50	1.000	3.522	+9
55	0.919	3.237	0
60	0.852	3.001	-7

The $SCOP_{HPS}$ of the MRC can deviate from +3.3% to -16.7%. In the best and worst case, the energy costs in the first year under consideration are 1,524 € and 1,851 €, respectively, compared to the gas costs of the GCB of 1,628 €.

The SCOP depends, among others, on the proportion of DHW in the total heat demand (y), the coverage of the HP in mono-energetic operating mode in terms of space heating and DHW (α) as well as different correction factors ($F_{\Delta\vartheta}$=1, F_ϑ, F_p=1.035 for preliminary planning, F_1 as well as F_2=0.764 for storage tanks with internal heat exchanger).

If F_P is not selected for the preliminary planning when calculating the $SCOP_{HPS}$ but instead is calculated using the power of the heat source circulation pump (95 W [20]) in the MRC, the $SCOP_{HPS}$ increases by 2.7%. However, the power of the heat source circulation pump is not always included in the manufacturer data sheets.

In GeoWPSys+Web, complex relationships in the design of GSHPS can be displayed and analyzed. For example, the nominal capacity of the HP and the length of connected BHE can be dimensioned smaller if the HP is operated in a mono-energetic operating mode instead of a monovalent operating mode.

The coverage ratio of the heating element has a significant impact on the HP's $SCOP_{HPS}$ (see Table 6) and, thus, on its electric power requirement, annual energy costs, CO_2 emissions and the primary energy of the overall system (see Figures 3 and 4).

DOI: 10.53196/gtj-2023.1

$$\mathrm{SCOP}_{HPS} = \frac{1}{(1-y)\cdot\frac{\alpha}{SCOP_h} + y\cdot\frac{\alpha}{SCOP_{DHW}} + 1 - \alpha} \quad (5)$$

$$\mathrm{SCOP}_h = \frac{COP \cdot F_{\Delta\vartheta} \cdot F_{\vartheta}}{F_P} \quad (6)$$

$$\mathrm{SCOP}_{DHW} = \frac{COP \cdot F_{\Delta\vartheta} \cdot F_1 \cdot F_2 \cdot F_{\vartheta}}{F_P} \quad (7)$$

Table 5: $SCOP_h$, $SCOP_{DHW}$ and $SCOP_{HPS}$ of different T_h und T_{DHW} settings and the percentage deviation of $SCHOP_{HPS}$ for the MRC

T_h	T_{DHW}	$SCOP_H$	$SCOP_{DHW}$	$SCOP_{HPS}$	%
30	55	5.361	3.237	4.664	3.3
35	50	5.109	3.522	4.634	2.6
35	55	5.109	3.237	4.515	0
35	60	5.109	3.001	4.405	-2.4
40	55	4.853	3.237	4.358	-3.5
45	55	4.597	3.237	4.196	-7.1
50	55	4.336	3.237	4.025	-10.8
55	55	4.067	3.237	3.843	-14.9
55	60	4.067	3.001	3.763	-16.7

Table 6 Impact of the choice of the HP device on the $SCHOP_{HPS}$ of the reference case (α: annual coverage of the HP in the annual heat supply; ξ: performance share of the HP nominal heating power (B0/W35) based on the standard heat load)

Name	ξ	α	$SCOP_{HPS}$	%
WPF 13 M	>1	1	4.515	0
WPC 07	0.750	0.985	4.523	0.2
WPF 07	0.750	0.985	4.523	0.2
WPC 05	0.582	0.9528	4.037	-10.6
WPC 04	0.477	0.9016	3.320	-26.5

DOI: 10.53196/gtj-2023.1

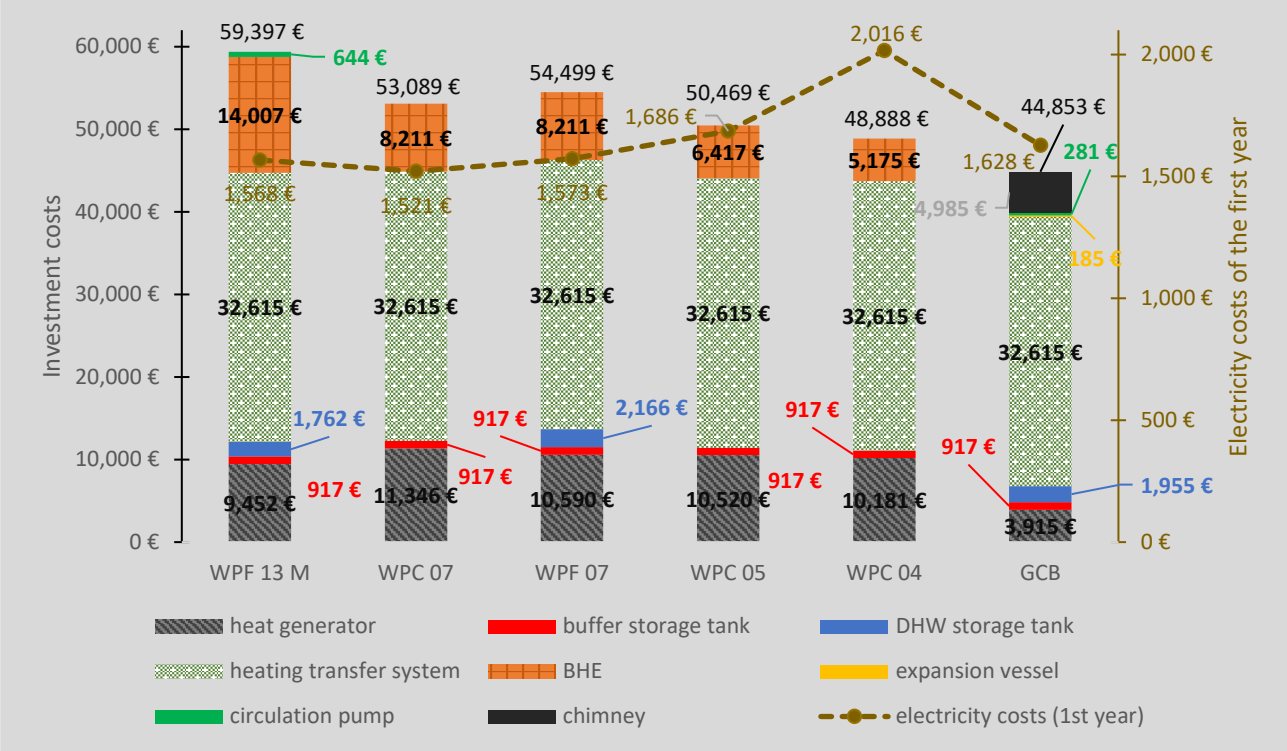

Figure 3: Investment costs (divided according to components) of various mono-energetic GSHPS compared to the MRC and a GCB

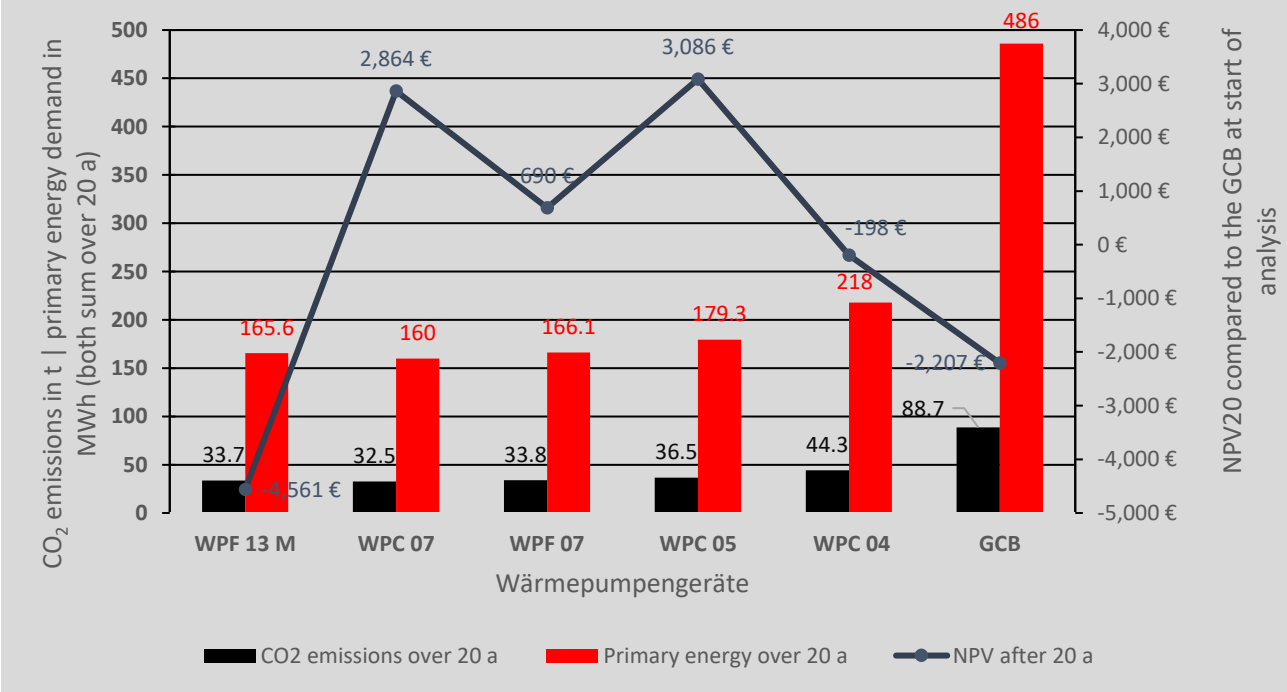

Figure 4: CO_2 emissions and primary energy demands summed over 20 years as well as the NPV20 of the MRC and mono-energetic system variants compared to the GCB at start of analysis (based on [1])

DOI: 10.53196/gtj-2023.1

The mono-energetic system with the HP WPC 04 has a heating element share of almost 10%. This reduces the $SCOP_{HPS}$ by 26.5% to a value of 3.32 (see Table 6) and the required BHE length to 119 m compared to 203 m for the monovalent system.

The reduced BHE length and the choice of a smaller HP device also reduce the investment costs for the overall system. The investment costs of the heating transfer system (floor heating), the heat generator and the BHE account for the largest proportion of the investment costs. The share of investment costs for the floor heating system in the total investment costs for the system variants considered amounts to an average of 63%.

On the other hand, the annual electricity costs of the HP rise with the increasing heating element's share of coverage. The HPs of the type WPC have integrated DHW storage tanks. Thus, the DHW storage investment costs and DHW storage heating losses for these HP types do not have to be applied. As a result, the WPF HP types also have lower NPVs compared to the WPC types of the same size (WPF 07 vs. WPC 07).

Furthermore, the NPVs after 20 years compared to the GCB at start of analysis (NPV20) decreases with smaller HPs due to the increasing proportion of heating element.

Figure 5 shows the NPV diagram of the MRC and the HP WPC 04 for the mono-energetic case. In the 16th year of operation, the NPV curve of the WPC 04 is above the curve of the GCB. Thus, the mono-energetic system is more economical than the GCB. The amortization point for the monovalent variant is in almost 27 years. In this form of representation, negative NPVs do not mean that the GSHPS will not amortize.

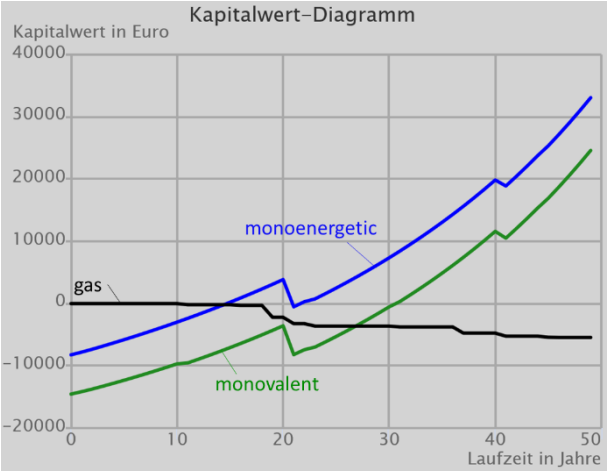

Figure 5: NPV diagram (screenshot of GeoWPSys+Web) of the reference case (monovalent (green) = WPF 13 M; mono-energetic (blue) = WPC 04)

In principle, the choice of the specific HP device and its boundary conditions with regard to other components (e.g. integrated DHW storage tanks) definitely have an influence on the economic efficiency, the CO_2 emissions and the primary energy demands.

The global crises in the recent years have shown that energy prices and cost increases

DOI: 10.53196/gtj-2023.1

are difficult to predict. Nevertheless, assumptions have to be made in order to estimate the profitability of projects for a future period. In the reference case, energy prices as well as the investment costs for HPs, other components of the GSHPS and the installation of BHE of the year 2021 are used.

Profitability analyses depend on a large number of parameters. The annual energy demand and the standard heating load of the building, the electricity and gas prices and their price increases, the investment costs and the calculation interest rate as well as government subsidies on the investment costs have a major influence [21].

Table 7 shows the effects on the NPV20 and on the amortization times of the HP WPF 13 M for different energy prices in the period from the year 2021 to 2023. The corresponding NPV diagrams of GeoWPSys+Web also show considerable differences due to the various price sets (see Figure 6).

If a 20% discounted HP electricity tariff of 25.58 ct/kWh and a blocking time of two hours are applied in the energy price set (a), the amortization period is reduced by six years compared to the original variant (a). The RHPC increases from 10.517 kW to 11.473 kW, however, this does not change the HP selection. Larger sized buffer and DHW storage tanks to bridge the blocking times are neglected in this consideration.

In addition, the variation of the future CO_2 price increase rate (starting in the year 2026) also has a strong impact on the curve shapes and the amortization times (see Figure 7). Higher CO_2 price increase rates favor the economic efficiency of the GSHPS in comparison to the GCB.

In buildings with high heating demands and heating loads, bivalent systems with a GCB can currently also be economically reasonable [21]. The profitability depends on the CO_2, gas and electricity prices and their increases [21]. With regard to the ecological evaluation criteria, the use of a fossil heat generator must be avoided.

In GeoWPSys+Web, it is possible to reduce the primary energy factors and CO_2 equivalents of electricity and gas for each year of observation. For example, the reduction of the annual CO_2 equivalent simulates an increased feed-in of renewable electricity into the power grid in the future (see Table 8). With increasing CO_2 reduction rates, the CO_2 emissions of the system decrease.

DOI: 10.53196/gtj-2023.1

Table 7: Effects on the NPV20 of the MRC for different energy prices

Prices	NPV20	Amortization time in years
Reference case (prices of 2021): gas 6.65 ct/kWh [22]| electricity 30.73 ct/kWh [23])	-4,561 €	29
Prices of 2022: gas 16.03 ct/kWh [22]| electricity 43.02 ct/kWh [23]	20,198 €	9
Actual prices (31.08.2023): gas 12.5 ct/kWh [22] | electricity 30.19 ct/kWh [23]	16,419 €	10
Highest gas price (01.09.2022): gas 40.41 ct/kWh [22]| electricity 54.6 ct/kWh [23]	98,295 €	3

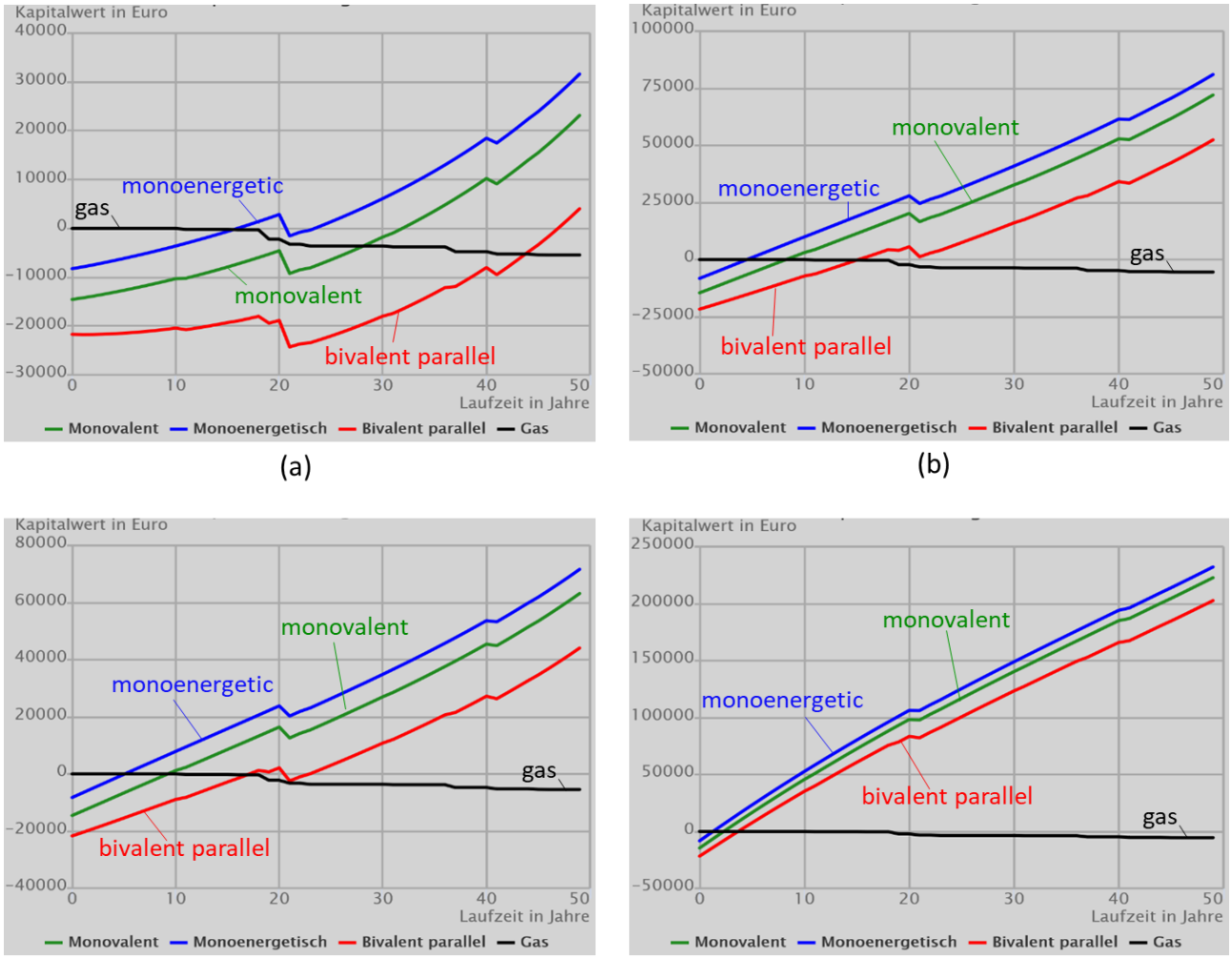

Figure 6: NPV diagrams of the reference case (monovalent (green) = WPF 13 M; mono-energetic (blue) = WPC 07; bivalent parallel (red)) for different energy price sets (a: prices of 2021 (reference case); b: prices of 2022; c: actual price (31.08.2023); d: highest gas price (01.09.2022)) out of GeoWPSys+Web

DOI: 10.53196/gtj-2023.1

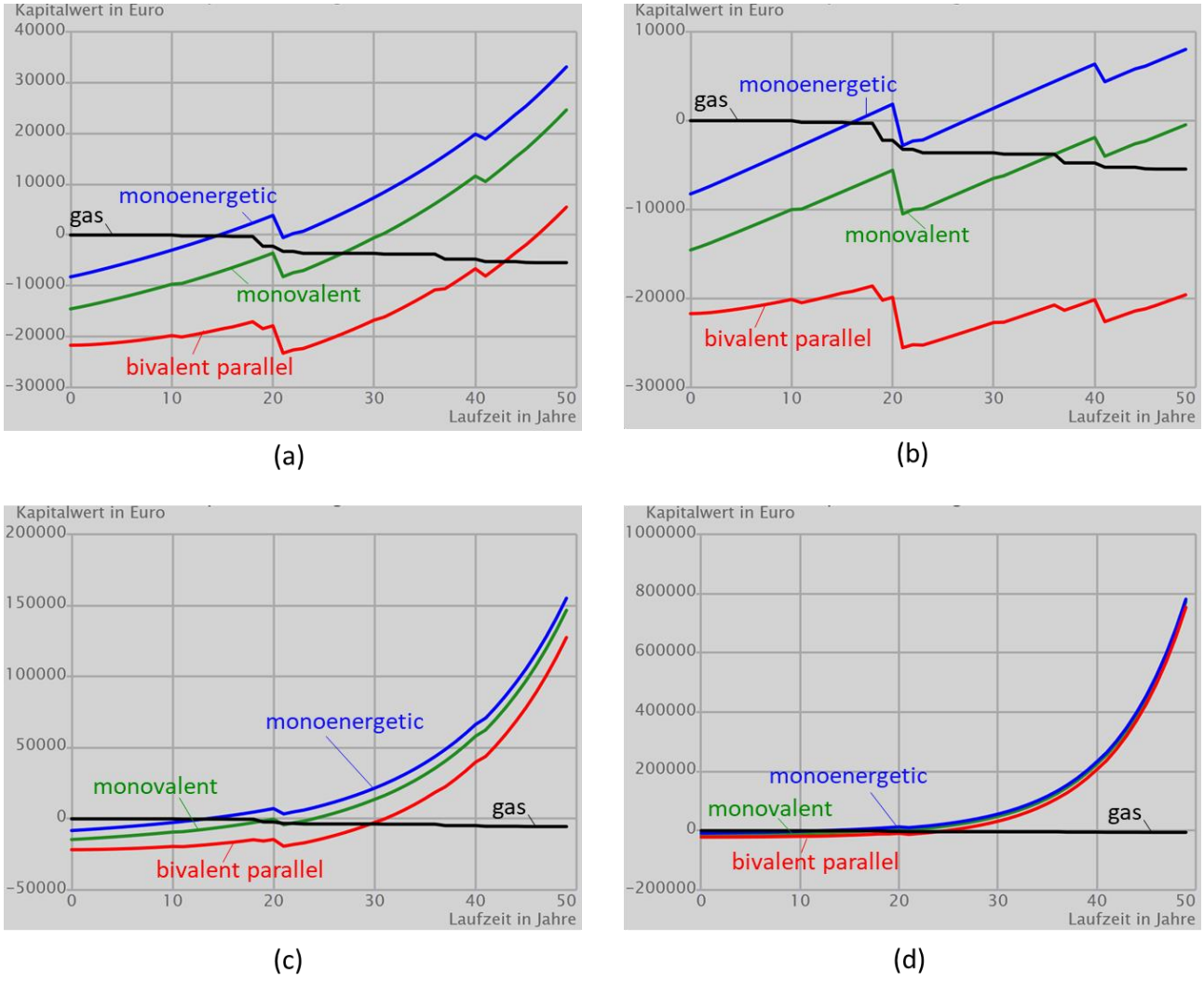

Figure 7: NPV diagrams of the reference case (monovalent (green) = WPF 13 M; mono-energetic (blue) = WPC 07; bivalent parallel (red)) for different annual CO_2 price increase sets (a: 10% (reference case); b: 5%; c: 15%; d: 20%) out of GeoWPSys+Web

Table 8: Effects on the sum of the CO_2 emissions over 20 years ($CO_2$20) of the MRC for different annual CO_2 equivalent decrease rates of the German electricity mix (CO_2eqEl)

CO_2eqEl in %	$CO_2$20 in t
0	33.66
1	30.65
3	25.60
5	21.60
10	14.79

DOI: 10.53196/gtj-2023.1

DISCUSSION AND OUTLOOK

The profitability and the ecological evaluation parameters are highly dependent on the building's energy demand and on the $SCOP_{HPS}$. Thus, the analyses have to be building-specific and component-specific. Economic savings of a GSHPS compared to a GCB mainly depends on the investment costs and the differences in annual energy costs. Latter are in turn dependent on energy prices and their increases. As seen in recent years, forecasts for price increases are subject to a high level of uncertainty. Consequently, price increases should be varied in economic analyses. Regarding the investment costs, catalog prices of 2021 and no end customer prices were used for the devices. The coupling of ModHPS to GeoWPSys+Web allows the verification of important planning parameters, e.g. the $SCHOP_{HPS}$ and coverage ratios. In future work, the effects of bidirectional coupled HP and subsurface simulations on the different evaluation parameters and on the design of the overall system, especially on the calculated size of the BHE, will be investigated.

GeoWPSys+Web is currently being further developed within the project GeoWaermeWende (FKZ: 03EN3059A) [24] with regard to the planning of geothermally fed low temperature district heating and cooling networks.

REFERENCES

[1] Weck-Ponten, S. (2023): Simulationsbasiertes Mehrebenen-Planungswerkzeug für geothermische Wärmepumpensysteme; Institute of Energy Efficiency and Sustainable Building E3D, RWTH Aachen University, dissertation 2023

[2] Blum, P.; Campillo, G.; Kölbel, T.: Techno-economic and spatial analysis of vertical ground source heat pump systems in Germany. In: Energy 36 (2011), pp. 3002-3011

[3] Casasso, A. and Sethi, R.: Efficiency of closed loop geothermal heat pumps: A sensitivity analysis. Renewable Energy 62 (2014), pp. 737-746

[4] Huang, S.; Ma, Z.; Cooper, P.: Optimal design of vertical ground heat exchangers by using entropy generation minimization method and genetic algorithms. Energy Conversion and Management 87 (2014), pp. 128–137

[5] Robert, F. and Gosselin, L.: New methodology to design ground coupled heat pump systems based on total cost minimization. Applied Thermal Engineering 62 (2014), pp. 481-491

DOI: 10.53196/gtj-2023.1

[6] Huang, S.; Ma, Z.; Wang, F.: A multi-objective design optimization strategy for vertical groundheat exchangers. Energy and Buildings 87 (2015), pp. 233-242

[7] Samson, M.; Dallaire, J.; Gosselin, L.: Influence of groundwater flow on cost minimization of ground coupled heat pump systems. Geothermics 73 (2018), pp. 100-110

[8] Casasso, A. and Sethi, R.: Sensitivity analysis on the performance of a ground source heat pump equipped with a double U-pipe borehole heat exchanger. Energy Procedia 59 (2014), pp. 301 – 308, European Geosciences Union General Assembly 2014, EGU 2014

[9] Sivasakthivel, T.; Murugesan, K.; Sahoo, P.K.: Optimization of ground heat exchanger parameters of ground source heat pump system for space heating applications. Energy 78 (2014), pp. 573-586

[10] Sivasakthivel, T.; Murugesan, K.; Thomas, H.R.: Optimization of operating parameters of ground source heat pump system for space heating and cooling by Taguchi method and utility concept. Applied Energy 116 (2014), pp. 76–85

[11] Esen, H. and Turgut, E.: Optimization of operating parameters of a ground coupled heat pumpsystem by Taguchi method. Energy and Buildings 107 (2015), pp. 329-334

[12] Madessa, H.B.; Torger, B.; Bye, P.F.; Erlend, A.: Parametric study of a vertically configured ground source heat pump system. Energy Procedia 111 (2017), pp. 1040-1049, 8th International Conference on Sustainability in Energy and Buildings, SEB-16, 11-13 September 2016, Turin, ITALY

[13] Han, C. and Yu, X.: Sensitivity analysis of a vertical geothermal heat pump system. Applied Energy 170 (2016), pp. 148-160

[14] VDI 4645: Heizungsanlagen mit Wärmepumpen in Ein- und Mehrfamilien-häusern – Planung, Errichtung, Betrieb. 2018. – Verein Deutscher Ingenieure, VDI-Richtlinie

[15] Weck-Ponten, S.; Eyhusen, D.; Frisch, J.; van Treeck, C.: Systemkonfigurator zur Dimensionierung mono- und bivalenter Wärmepumpen: Teil 1: Systemkonfigurator und Eingabeparameter. In: HLH-VDI Fachmedien 72 (2021), no. 01-02, pp. 42–46. http://dx.doi.org/10.37544/1436-5103-2021-01-02-42

[16] VDI 4640 Blatt 2: Thermische Nutzung des Untergrunds – Erdgekoppelte Wärmepumpen-anlagen. 2019. – Verein Deutscher Ingenieure, VDI-Richtlinie

[17] VDI 2067 Blatt 1: Wirtschaftlichkeit gebäudetechnischer Anlagen- Grundlagen und Kostenberechnung. 2012. – Verein Deutscher Ingenieure, VDI-Richtlinie

[18] Weck-Ponten, S.; Frisch, J.; van Treeck, C.: Simplified heat pump system model integrated in a tool chain for digitally and simulation-based planning shallow geothermal systems. In: Geothermics 106 (2022), 102579. http://dx.doi.org/10.1016/j.geothermics.2022.102579 – ISSN 0375–6505

[19] VDI 4650 Blatt 1: Berechnung der Jahresarbeitszahl von Wärmepumpenanlagen. 2019. – Verein Deutscher Ingenieure, VDI-Richtlinie

[20] JAZ-Rechner des BWP: https://www.waermepumpe.de/jazrechner/, zuletzt abgerufen am 12.10.2023

[21] Weck-Ponten, S.; Eyhusen, D.; Frisch, J.; van Treeck, C.: Systemkonfigurator zur Dimensionierung mono- und bivalenter Wärmepumpen: Teil 2: Parameterstudien und Ergebnisse. In: HLH-VDI Fachmedien 72 (2021), no. 3, pp. 45–49. http://dx.doi.org/10.37544/1436-5103-2021-03-45

[22] Aktuelle Gaspreise für Neukunden: https://www.verivox.de/gas/gaspreise/, zuletzt abgerufen am 12.10.2023

[23] Aktuelle Strompreise für Neukunden: https://www.verivox.de/strom/strompreisentwicklung/, zuletzt abgerufen am 12.10.2023

[24] Drexler, L; Cuypers, L.; Weck-Ponten, S.; Lemmerz, T.; Moubayed, F.; Förderer, A.; Becker, R.; Frisch, J.; Fuentes, R.; Blankenbach, J.; van Treeck, C.: GeoWaermeWende - Empowering Low-Temperature District Heating and Cooling Networks with Comprehensive Geospatial Monitoring, Multi-Purpose Simulation Approaches and User-Centric Planning Tools. In: geoTHERM Journal. 2023

DOI: 10.53196/gtj-2023.1

APPENDIX

Table 4: Boundary conditions of the reference case

Parameter	Value
Building type	New building
Standard building heat load	10 kW
Annual energy demand for heating | DHW	15,372 kWh | 4,530 kWh
Heating limit temperature	15 °C
Blocking times	0 h
RHPC	10.52 kW
HP device (monovalent case)	WPF 13 M
Nominal capacity of the HP device (B0/W35)	12.98 kW
COP of the HP device (B0/W35)	4,57
Supply temperatures for heating | DHW	35 °C | 55 °C
Buffer storage tank	SBP 200 E
DHW storage tank	SBB 400-1 Plus
Type of thermal heat transfer system	Floor heating
Floor heating area	181 m²
Investment costs floor heating system	32,615 €
Specific BHE heat extraction rate	50 W/m²
BHE length	203 m
Specific Investment costs BHE	69 €/m
Total investment costs of the monovalent GSHPS	59,397 €
Total investment costs of the GCB system	44,852 €
CO_2 equivalents: electricity | gas	366 g/kWh |201 g/kWh
Type of electricity tariff	Domestic electricity tariff
Variable portion | annual basic costs of the electricity tariff	32 ct/kWh | 155 €
Price increase of the electricity tariff (variable portion)	2%
Variable portion | annual basic costs of the gas tariff	6.65 ct/kWh | 160 €
Price increase of the gas tariff (variable portion)	3%
Price increase o the CO_2 price	10% (from the year 2025)
Calculation interest rate	5%

DOI: 10.53196/gtj-2023.1

Why should Oil and Gas go Geothermal? A Risk Assessment

Henning VON ZANTHIER, LL.M.

VON ZANTHIER & DACHOWSKI

D-10719 Berlin

1. ABSTRACT

Rapid climate change and the aim to achieve the 1.5 degrees Celsius target mean that the business model of the Oil and Gas industry (O+G) is becoming risky. The energy sector accounts for more than 70 % of global CO_2 emissions and if the use of oil, gas and coal stopped tomorrow, we would have solved the climate crisis, but would have a giant economic crisis.

Preventing both, an economic and a climate crisis, there is a solution:

O+G could transform its business model naturally by turning into the geothermal sector, which is in its technical skills and its assets very close to O+G. O+G could also provide the urgently needed financing for geothermal energy.

However, the Oil and Gas companies are still hesitant to undergo a radical transformation, possibly underestimating the strong climate-friendly policies against their traditional business model, which can be brought about by the radical climate changes already in the 2030s.

Germany could establish a political and an economic framework encouraging O+G to turn to geothermal which then other countries could follow. If O+G changes then to geothermal, the communities need less finance to pay and all citizens enjoy a less polluted planet.

Key words: Oil and Gas, Geothermal, Climate change, Political framework, CO_2 Emissions.

DOI: 10.53196/gtj-2023.1

2. OUTSET

In the face of rapid climate changes, it has become a priority of many countries to limit CO_2 emissions to achieve the 1.5 degrees Celsius target set in the Paris Climate Agreement. Global energy-related CO_2 emissions has reached ca. 37 billion metric tons in 2022.[1] However, to reach the target of less than 1.5 degrees Celsius of global warming, we need to reduce those emissions to 16 billion metric tons of CO_2 p.a. till 2030.[2] According to a study published by McKinsey, 90 % of our current global population lives in areas which by 2099 will be uninhabitable if a temperature increase of 3-4 degrees Celsius were to happen as it seems today.[3]

According to a study by the International Panel on Climate Change, we have 6.5 years left to limit global warming to 1.5 degrees Celsius.[1] Tipping points are expected latest in the 2030s, when 1.5 degrees is reached, and the climate risks might accumulate and climate damages are unpredictable.[2] Then, strong national countermeasures towards CO_2 emissions are likely.

There is hope on the horizon: The electricity production by fossil fuels decreased from 2022 to 2023 in the EU by 17 %,[4] which will alarm the fossil industry: Once the trend of decay of fossils is clear, O+G will create an avalanche of shift from fossil to renewable, in order to get the lowest hanging fruits of renewables and thus save their assets as far as possible. This could be the last resort to save the 1.5 Celsius goal of the Paris accord 2015.

3. RISKS OF OIL AND GAS INDUSTRY

O+G is risky because it is responsible for a very significant proportion of the said global emissions. Ca. 70 % of global greenhouse gas emissions come from energy sector and 40 % of global greenhouse gas emissions come from O+G industry.[5] Therefore it may be one of the first sectors targeted by the climate-friendly policies on national and international level. As the covid pandemic 2020-2022 has shown, national governments can react very quickly and strongly when it comes to natural disasters. Ultimately, radical measures are also possible, such as a possible complete ban on CO_2 emissions. A similar radical move in the

[1] "CO2 Emissions in 2022", IEA, 2023, Paris, https://www.iea.org/reports/co2-emissions-in-2022,
[2] "Global Energy Perspective 2022", McKinsey&Company, 2022,
[3] Earlybird Analysis 2021, McKinsey Global Institute 2020, Zeit 2019,
[4] https://www.zeit.de/politik/ausland/2023-08/eu-stromerzeugung-fossile-brennstoffe-erneuerbare-energien, access: 11.09.2023,
[5] https://ourworldindata.org/emissions-by-sector,access: 21.02.2023,

DOI: 10.53196/gtj-2023.1

face of a great risk was the stop of car production in the USA during WW2 to produce military equipment. Alternatively, it is possible that because of climate-friendly policies the demand for oil and gas will dramatically fall in the 2030s. Therefore, the quicker O+G leave fossil fuels for renewable sources of energy, the lesser these risks will be.

4. WHY CAN GEOTHERMAL ATTRACT THE OIL AND GAS INDUSTRY?

A viable option for the Oil and Gas Industry can be a turn to geothermal energy. That is primarily because of the similarities between the two sectors. Much of the work of geothermal exploration (possibly up to 90 % in hydrogeothermal systems) is like O+G, including geology and drilling, equipment for drilling, seismic, chemical aspects, and mapping & resource allocation. The main differences are heat exchange, power production and energy distribution. O+G could therefore still make use of their experts and know-how in the new industry what would also give them a kick-start as regards other competitors on the market.

An example of a successful transition in that area is A.P. Moller-Maersk A/S, a Danish company who has completely abandoned O+G some 7 years ago and has decided to set up a company, Innargi A/S, solely for the purpose of the development of geothermal energy projects.

Currently in the geothermal sector there are also many other pioneers (without an O+G background). For example, there is German Vulcan Energie Ressourcen GmbH, a company which is working on an innovative solution of acquiring lithium from the geothermal brine. Canadian Eavor Technologies Inc. is developing petrothermal energy for heat and power, a new technology, which is still tested in e.g., Geretsried, Bavaria.[6] As it can be seen, the geothermal industry is already developing quickly but the change could be even more significant if the O+G were to put their resources into the geothermal sector.

Another reason for the O+G to move to geothermal sector is that the geothermal industry could be shaped like the O+G from an economic perspective and thus become more attractive for O+G. The business model of O+G is based on spread investments with industrialized large-scale projects all over the globe, where one project benefits from the experiences from many former projects.

[6] https://www.thinkgeoenergy.com/drilling-starts-for-first-commercial-eavor-loop-in-geretsried-germany/, access: 07.09.2023,

DOI: 10.53196/gtj-2023.1

Currently, the geothermal sector is scattered, and it is uncommon that one company owns more than one or maximum a few geothermal plants, thus initial mistakes can repeat and the overall experience of the project developer is often limited and thus costs for traditional geothermal projects are often higher than if they would have been performed by O+G on a large scale. Geothermal companies with large scale projects coming from O+G, like Innargi, do normally not ask e.g. for subsidies or state backed exploration risk insurances and thus can be profitable without subsidies, because the costs of a futile borehole can be balanced by the success of the other borehole by large scale and the lesser costs of an integrated geothermal system with a lot of experiences of former projects. One of the reasons for this phenomenon is lack of know-how of the company owners who are very often local authorities or local utilities and get often experiences from one project, but cannot built on former experience of other projects

A comprehensive management of the coordination of geology, drilling and later maintenance of the boreholes, which have been experienced in many former projects reduces systemic mistakes, which might occur, if different subcontractors work on these different fields in smaller projects or do it for the first time.

O+G, with its vast resources, could create a scalable industrialized model of business just like it did in their own sector. That way, the geothermal sector could potentially become much more professional and profitable on a large scale. That is what the pioneer companies like Vulcan, Eavor and Innargi are trying to do. Should they succeed, the geothermal sector will be a real alternative for the O+G sector not only in technical, but also in economic terms.

5. WHY IS OIL AND GAS INDUSTRY STILL ATTRACTIVE DESPITE OF THESE RISKS?

It is remarkable that despite those risks, O+G still does not think about a complete transition to renewable sources of energy. One of the reasons for it may be that O+G has always been profitable. For 50 years, O+G has been making 2.6 billion USD profit a day.[7] In fact, many new investments regarding developing new oil and gas fields are expected – according to studies, up to 570 billion USD p.a. will be spent on new oil and gas development and exploration by 2030.[3] Such new fossil fuel investments

[7] https://www.theguardian.com/environment/2022/jul/21/revealed-oil-sectors-staggering-profits-last-50-years, access: 21.02.2023,

DOI: 10.53196/gtj-2023.1

might provoke strong countermeasures by national governments in the 2030s if climate changes dramatically.

Another reason may be that big companies are occasionally sleepwalkers to disruptive changes. A good example of that is Kodak, once a worldwide producer of photography equipment. In 2005 the company still had a turnover of 12 billion USD, but it missed the digital revolution and the development of smartphones made Kodak go bankrupt in 2012.[8]

Another example is the German car industry. E.g., Volkswagen Group paid over € 30 billion in fines and indemnifications before changing to electric cars.[9] Big companies can apparently sometimes miss its chance to transition until it is too late.

6. PROPER RISK ASSESSMENT GIVES NATURAL RISKS PRIORITY OVER POLITICS

It is however untrue to say that O+G do not think about a transformation at all.

O+G has in Germany and the EU successfully lobbied for hydrogen as the "backbone" of the energy transformation, since at least gas is supposed to serve for quite some decades for the production of hydrogen, even though in climate terms hydrogen wastes up to 40 % of power and is not sufficiently available and thus is rather a niche product for high temperature and heavy vehicles than the "backbone" of the energy transformation.[10]

O+G is already changing and is aware of the risks of the climate change. Many big Oil and Gas companies in fact have already started investing in geothermal projects. In the face of the rapid climate changes those decisions are, however, not enough. As mentioned before, we now need radical moves and cuts on CO_2 emissions, otherwise we may face severe climate consequences already in the 2030s. Many industries prefer to ignore scientific prediction of natural disasters and believe in the present political framework in their risk assessments. This assessment is wrong since it is nature and its interpretation that set the ultimate framework for the risks and not politics with their current measures.

A good example of the unreliability of current politics for future risks can be seen in Poland where the government introduced in 2016

[8] https://www.independent.co.uk/news/business/analysis-and-features/the-moment-it-all-went-wrong-for-kodak-6292212.html, access: 07.09.2023,
[9] https://www.bbc.com/news/business-61581251, access: 14.02.2023,
[10] https://www.weforum.org/agenda/2021/08/hydrogen-carbon-intensive-energy-solution/,access: 07.03.2023,

DOI: 10.53196/gtj-2023.1

legislation which almost completely stopped the development of wind energy for years in Poland trying to favor "Polish" coal. However, in the face of growing energy prices by coal and the dissatisfaction of the citizens with the air pollution, the Polish government withdrew the legislation, stopping renewable energy. [11]

The predicted radical natural changes in the 2030s can therefore leave other governments with no option but to rapidly tighten the CO2 emissions laws.

7. GERMANY AS A POSSIBLE TRENDSETTER

Germany could play a crucial role in encouraging O+G to move to Geothermal. The country is the 7th worst CO_2 polluter in the world, but it is responsible "only" for 2 % of the world emissions.[12] At first sight it cannot therefore bring a radical change and contribute to limiting the CO_2 emissions globally. However, it could establish a market design for O+G to stop new investments in Oil and Gas and instead to put that money into geothermal energy. That way Germany could not only contribute to lowering its own emissions but in fact affect the global energy emissions (ca. 40 % of the global total emissions).[13]

Germany has already published a Cornerstone Paper in November 2022 which includes several changes which should simplify investments in the geothermal sector. For example, geothermal procedures should be accelerated, open access to geological and geothermal data should be granted and subsidies should be available. However, those changes are not enough. In fact, some O+G are not very keen on subsidies. Arguably, a better solution would be to install tax holidays for RES investments (a similarity to the US Inflation Reduction Act 2022). That way the German government could approach and communicate with O+G on transformation and all investment risk would stay with Oil and Gas. Moreover, tax holidays are often cheaper than subsidies.

If Germany and then other governments adopt that model, a leverage of 20 in CO_2 reduction could be possible. (from max 2 % of CO_2 emissions within Germany to max 40 % on the planet). That way, together with phasing out coal, a drastic reduction of CO_2 emissions on a global level could be possible.

[11] https://notesfrompoland.com/2023/02/09/polish-parliament-approves-law-to-unblock-building-of-onshore-wind-farms/, access: 07.09.2023,

[12] https://www.statista.com/statistics/271748/the-largest-emitters-of-co2-in-the-world/,access: 07.09.2023,

[13] https://ourworldindata.org/emissions-by-sector,access: 21.02.2023,

DOI: 10.53196/gtj-2023.1

8. IF OIL AND GAS CHANGE TO GEOTHERMAL, THEY OFFER 3 BENEFITS FOR OTHER STAKEHOLDERS

If O+G changes to geothermal, they offer 3 benefits for other stakeholders.

First, the energy production industry would profit from the financial means and skills of O+G. That is because Oil and Gas would bring the capital, the geological know-how and the drilling experience for establishing geothermal plants. That way the global development of geothermal energy could really accelerate.

The second beneficiary of a said transition would be the communities and cities. Outsourcing the development of geothermal plants to big Oil and Gas companies would mean that cities and utilizes could save their liquidity and take advantage of the much broader knowledge of the exploration and drilling risk of O+G. Furthermore, using the contracting system would mean that the control over the plants would be given back from O+G to cities when the investment is paid off. That way communities and cities could avoid financial and geological risks connected to geothermal energy while still benefiting from it.

Finally, the transition of big Oil and Gas companies to Geothermal would be profitable for all citizens, as geothermal energy production does not pollute the climate anymore and therefore it could significantly contribute to the reduction and ultimate elimination of climate change and the air pollution in the cities.

9. CONCLUSIONS OF THE RISK ASSESSMENT

If big Oil and Gas integrate the time scale of the climate risks it is likely that their traditional business model will not allow new Oil and Gas plants and investments. Strong measures of national governments against CO_2 emissions in the 2030s are likely if climate disasters occur. Geothermal is the best way to reduce these risks of O+G. The German government has the chance to create a market design to not only reduce CO_2 emissions in Germany (2 % of global emissions) but also by its market design to attract big Oil and Gas to investment into geothermal, thus facilitating a reduction of up to 40 % in global CO_2 emissions by the energy sectors.

10. BIBLIOGRAPHY

[1] Masson-Delmotte, V., P. Zhai, H.-O. Pörtner, D. Roberts, J. Skea, P.R. Shukla, A. Pirani, et al.

DOI: 10.53196/gtj-2023.1

(2018): „Global Warming of 1.5°C. An IPCC Special Report on the impacts of global warming of 1.5°C", Cambridge University Press, Cambridge, UK and New York, NY, USA, 2018.

[2] T. Lenton, J. Rockström, O. Gaffney, S. Rahmstorf, K. Richardson, W. Steffen & H. Schellnhuber (2019): „Climate tipping points – too risky to bet against", **Nature,** 575, 2019, pp. 592-595.

[3] B. Kursk, O., G. Muttitt, A. Picciarello, L. Dufour, T. Van de Graaf, A. Goldthau, D. Hawila, et al. (2022): „Navigating Energy Transitions: Mapping the Road to 1.5°C.", International Institute for Sustainable Development (IISD).

DOI: 10.53196/gtj-2023.1